

Mapping the
physico-chemical
properties of mineral
dust

P. Formenti et al.

Mapping the physico-chemical properties of mineral dust in western Africa: mineralogical composition

P. Formenti¹, S. Caquineau², K. Desboeufs¹, A. Klaver¹, S. Chevaillier¹,
E. Journet¹, and J.L. Rajot^{1,3}

¹LISA, UMR CNRS 7583, Université Paris Est Créteil et Université Paris Diderot, Institut Pierre Simon Laplace, Créteil, France

²IPSL/LOCEAN, UMR 7159 – IRD – CNRS – UPMC – MNHN, Institut de Recherche pour le Développement, Bondy, France

³IEES, UMR IRD 242 – IRD – UPMC – CNRS – UPEC – AgroParisTech, Bondy, France

Received: 7 March 2014 – Accepted: 3 April 2014 – Published: 23 April 2014

Correspondence to: P. Formenti (paola.formenti@lisa.u-pec.fr)

Published by Copernicus Publications on behalf of the European Geosciences Union.

Title Page

Abstract

Introduction

Conclusions

References

Tables

Figures

⏪

⏩

◀

▶

Back

Close

Full Screen / Esc

Printer-friendly Version

Interactive Discussion

Abstract

In the last few years, several ground-based and airborne field campaigns have allowed exploring the properties and impacts of mineral dust in western Africa, one of the major emission and transport areas worldwide. In this paper, we explore the synthesis of these observations to provide with a large-scale quantitative view of the mineralogical composition and its variability with source region and time after transport.

This work reveals that mineral dust in western Africa is a mixture of clays, quartz, iron and titanium oxides, representing at least 92 % of the dust mass. Calcite ranged between 0.3 and 8.4 % of the dust mass depending on the origin. Our data do not show a systematic dependence of the dust mineralogical composition with origin, likely as in most of the cases they represent the composition of the atmospheric burden after 1–2 days after emission, when air masses mix and give raise to a more uniform dust load. This has implications for the representation of the mineral dust composition in regional and global circulation models, and satellite retrievals.

Iron oxides account for 58 ± 7 % of the mass of elemental Fe, and between 2 and 5 % of the dust mass. Most of them are composed of goethite, representing between 52 and 78 % of the iron oxide mass. We estimate that titanium oxides account for 1–2 % of the dust mass, depending on whether the dust is of Saharan or Sahelian origin.

The mineralogical composition is a critical parameter to estimate the radiative and biogeochemical impact of mineral dust. The results on dust composition have been applied to estimate the optical properties as so as the iron fractional solubility of Saharan and Sahelian dust.

Data presented in this paper are provided in numerical form upon email request while they are being implemented as a public database, the Dust-Mapped Archived Properties (DUST-MAP), an open repository for compositional data from other source regions in Africa and worldwide.

Mapping the physico-chemical properties of mineral dust

P. Formenti et al.

Title Page

Abstract

Introduction

Conclusions

References

Tables

Figures



Back

Close

Full Screen / Esc

Printer-friendly Version

Interactive Discussion



1 Introduction

Mineral dust from wind-driven soil erosion is an important player in the climate system. It is emitted in large quantities from arid and semi-arid regions of the globe, mostly Africa, Asia, Australia and North America (Shao et al., 2011), accounting for about 2000 Mt to the annual aerosol emissions at the global scale. Once in the atmosphere, mineral dust has several climatic and environmental impacts, related to its ability of scattering and absorbing radiation, both in the solar and terrestrial spectra, of acting as giant cloud and ice nuclei, of altering the concentrations of some gaseous pollutants (such as ozone), and of providing nutrients to the ecosystems via dry and wet deposition, whereby also changing the surface albedo (Shao et al., 2011; Mahowald et al., 2011).

The relevance of those phenomena can be expressed in terms of radiative forcing, whose magnitude, in terms of central values, is estimated to be as high as $0.5\text{--}1\text{ W m}^{-2}$ at the global scale (Mahowald et al., 2011).

Uncertainties remain however important, because of the spatial heterogeneity of concentrations, due to localized emission and short residence time in the atmosphere (1 week at the most, depending on particle size), but also because of the far from satisfactory knowledge on the underlying physico-chemical properties, composition, size and shape, ruling the optical, chemical and physical interactions of mineral dust with radiation and the atmospheric/terrestrial/oceanic constituents (Formenti et al., 2011a). This is particularly the case of the composition. Dust is made of different minerals, whose proportions, at emission, depend on the mineralogy of the source region and surface wind speed relative to the soil roughness, which determines their size distribution (Marticorena and Bergametti, 1995; Alfaro et al., 1998). The various minerals, clays, quartz, potassic and sodic feldspars, calcium-rich carbonates and sulphates, iron and titanium oxides, have different mineralogical and crystallographic properties (Pye, 1987), therefore they may act differently with respect to light extinction, absorption of water, and surface reactivity. For example, iron oxides have been shown to control

ACPD

14, 10241–10310, 2014

Mapping the physico-chemical properties of mineral dust

P. Formenti et al.

Title Page

Abstract

Introduction

Conclusions

References

Tables

Figures

⏪

⏩

◀

▶

Back

Close

Full Screen / Esc

Printer-friendly Version

Interactive Discussion

Mapping the physico-chemical properties of mineral dust

P. Formenti et al.

Title Page

Abstract

Introduction

Conclusions

References

Tables

Figures

⏪

⏩

◀

▶

Back

Close

Full Screen / Esc

Printer-friendly Version

Interactive Discussion

the interaction with light in the UV-visible spectrum (Sokolik and Toon, 1999), whereas quartz, clays and Ca-rich carbonates become important when looking at the infrared part of the radiation spectrum (Sokolik et al., 1998). Clays but also feldspars come to play when it comes in investigating the capacity of dust of activating as ice nuclei at low temperature (Hoose et al., 2008; Atkinson et al., 2013), whereas calcite (calcium carbonate) shows high surface reactivity with respect to various atmospheric pollutants (Crowley et al., 2010). Another clay family, the smectites, bears the most soluble iron which might become available as nutrient to the marine phytoplankton (Journet et al., 2008). The properties of mineral dust are size-dependent, and the dimensional spectrum of mineral dust particles at emission extends over various orders of magnitude from approximately 200–300 nm to 100 μ m (Kandler et al., 2009) depending on wind speed at emission. As a consequence, the properties of mineral dust vary as a function of time after emission due to size-dependent deposition, mixing, and gaseous condensation. Because these processes are not well established, the physico-chemical properties of mineral dust have to be determined experimentally at the various times of their life cycle.

In this paper, we relate on the mineralogical and chemical composition at emission or at most within 1–2 days from emission of mineral dust over western Africa. The southern Sahara is the location of two of most persistent dust sources at the global scale, the Bodélé depression in between the Tibesti and the Ennedi mountain chains in Chad, and the areas in between the east of Mauritania, the North of Mali and the south of Algeria (Prospero et al., 2002; Laurent et al., 2008; Washington et al., 2006; Shao et al., 2011). These sources are relevant at the global scale as their emissions are transported across the Atlantic Ocean towards South and Central America (Reid et al., 2003; Koren et al., 2006; Ben-Ami et al., 2009, 2010).

The atmospheric content of mineral dust in western Africa shows a very pronounced seasonal cycle despite high variability, both at the daily and inter-annual scales (N'Tchayi et al., 1994; N'Tchayi Mbourou et al., 1997; Goudie and Middleton, 2001). This is largely explained by the alternance of two meteorological regimes. Through-

Mapping the physico-chemical properties of mineral dust

P. Formenti et al.

Title Page

Abstract

Introduction

Conclusions

References

Tables

Figures



Back

Close

Full Screen / Esc

Printer-friendly Version

Interactive Discussion



out the year, the “Harmattan”, a north-eastern dry wind, is responsible for intense dust emissions in the arid areas of the Sahara and very efficient transport towards the Atlantic Ocean and across the Sahel (Pye, 1987; Sokolik et al., 2001; Laurent et al., 2008). Wintertime is also the biomass burning season south of approximately 13° N (Haywood et al., 2008), and mixing between dust and biomass burning aerosols might occur during southward transport (Johnson et al., 2008). During summer, the Inter Tropical Convergence Zone (ITCZ) displaces northward, allowing the surface Monsoon flow to intrude the continent from the South-West towards the continental Sahel. This shift induces a progressive organization of convection from isolated cells to large-scale fast propagating systems, which, particularly at the beginning of the Monsoon season, are often not precipitating, and efficient in eroding bare soils (Abdourhamane Touré et al., 2011) and producing mineral dust. The summertime column dust content over western Africa results therefore from the superimposition of local emission from the Sahel and remote transport of dust emitted in the Sahara (Tegen and Fung, 1994; Yoshioka et al., 2005; Marticorena et al., 2010).

Because the soils of these two zones have different mineralogy (Pye, 1987; Claquin et al., 1999; Caquineau et al., 2002), mixing or layering of dust transported from the Sahara and locally emitted by convection over the Sahel should be detectable through differences in the composition over the atmospheric column.

Furthermore, western Africa is prone to land-use change because of the rapid demographic increase and desertification during drought periods (ECA, 2005; Dai, 2011), which could feedback in increased emission (Carslaw et al., 2010). Rajot (2001) have shown that, in the Sahel, additional emission by wind erosion of mesoscale meteorological disturbances, such as organized convective systems, occurs on harvested soils only. These additional emissions, anthropogenic in origin, are far from being well quantified but to date they are assumed to be within 20 % of the total emission at the global scale (Forster et al., 2007).

In this paper we report the synthesis of data from various aircraft and ground-based field campaigns which have taken place in western Africa in 2006 and 2007. These

Mapping the physico-chemical properties of mineral dust

P. Formenti et al.

Title Page

Abstract

Introduction

Conclusions

References

Tables

Figures

⏪

⏩

◀

▶

Back

Close

Full Screen / Esc

Printer-friendly Version

Interactive Discussion

are the African Monsoon Multidisciplinary Analysis (AMMA) Special Observing Period-0 (SOP0; Rajot et al., 2008), augmented of the airborne Dust and Biomass-burning Experiment (DABEX; Haywood et al., 2008), and Special Observing Period-1 and -2 (SOP1-2; Reeves et al., 2010); the Dust Outflow and Deposition to the Ocean (DODO; McConnell et al., 2008) and the Geostationary Earth Radiation Budget Intercomparison of Longwave and Shortwave radiation (GERBILS; Haywood et al., 2011).

These observational data on dust composition have been collected consistently through time, with respect to the air inlet and samplers, sampling protocols and analytical techniques. This allows comparing the results and investigating differences, similarities and trends, taking into account the artefacts, in particular those arising from different size cut-off of samplers, especially for aircraft sampling.

This paper provides with the quantitative estimate of the mineralogical composition of mineral dust at the regional scale. Some of the data discussed in this paper have been published previously (Formenti et al., 2008, 2011b; Klaver et al., 2011; Rajot et al., 2008; Formenti et al., 2013). Here, they are revisited with a broader perspective discussion of the mineralogical variability at the regional scale of western Africa and its implications for climate.

This paper discusses whether, when mapped at the scale of western Africa, the regional variability at emission deriving from the heterogeneity of the mineralogy of the parent soils is still relevant or whether it becomes irrelevant when dust is airborne. This is important for developing a model parameterisation for dust in regional and global climate models or for satellite retrieval algorithms.

2 Methods

Full details of the field campaigns operations, experimental procedures, collection and analytical protocols are described in a number of companion papers (Haywood et al., 2008, 2011; Formenti et al., 2008, 2011b; Rajot et al., 2008; McConnell et al., 2008, 2010; Klaver et al., 2011) which are resumed hereafter.

2.1 Field campaigns

The African Monsoon Multidisciplinary Analysis (AMMA) was an international project to improve our knowledge and understanding of the West African monsoon (WAM), its variability on daily-to-interannual time scales, and its effects on the status of the atmosphere (Redelsperger et al., 2006). Because of its links to precipitation, wind speed, soil surface state, and drought at different time scales, mineral dust aerosols play a role in this comprehensive scientific framework.

The experimental strategy of the AMMA program was based on embedded multi-year, seasonal and intensive observation periods (Janicot et al., 2008; Lebel et al., 2010). The observations used in this paper were conducted during the intensive observations periods, called Special Observing Periods (SOPs). The wintertime SOP (SOP0), was dedicated to the investigation of mineral dust and biomass burning, and their mixing, took place from 13 January and 13 February 2006. The summertime observations (periods SOP1 and SOP2) started on 31 May 2006 and ended on 17 July 2006 and were dedicated to the fine description of the interactions between aerosols and convection.

The ground-based observations were conducted at the AMMA supersite of Bani-zoumbou (13.5° N; 2.6° E, 250 m a.s.l.), located at a remote location at about 60 km east from the capital of Niger, Niamey. This site has been operational since the early 1990s, when the first measurements of soil erosion were performed on a cultivated field and a fallow (Rajot, 2001). Since 1995, the site is also an Aerosol Robotic Network (AERONET) station measuring columnar aerosol optical properties. The ground-based site operations are fully described in Rajot et al. (2008).

The aircraft observations were conducted from Niamey, Niger. The wintertime airborne campaign, called AMMA SOP0-DABEX, was conducted onboard the Facility for Airborne Atmospheric Measurements (FAAM) BAe-146 aircraft (Haywood et al., 2008). The aircraft performed thirteen research flights in the area between 8° and 18° N, including three dedicated excursion to the north of Niger, toward the Aïr Mountains and

Mapping the physico-chemical properties of mineral dust

P. Formenti et al.

Title Page

Abstract

Introduction

Conclusions

References

Tables

Figures

⏪

⏩

◀

▶

Back

Close

Full Screen / Esc

Printer-friendly Version

Interactive Discussion



the Ténéré desert to probe specifically mineral dust whilst transport. In summertime, the observations were conducted onboard the Service des Avions Français Instruments pour la Recherche en Environnement (SAFIRE) ATR-42, which operated twenty research flights in the area between 6° and 20° N, therefore crossing the ITCZ to the north to contrast the Sahara and the Sahelian dust properties in their respective boundary layers (Reeves et al., 2010; Formenti et al., 2011b).

The Geostationary Earth Radiation Budget Intercomparison of Longwave and Shortwave radiation (GERBILS) found its scientific motivation in the discrepancy that had been found between the satellite observations and the numerical weather model predictions of the top of the atmosphere outgoing longwave radiation over desert areas in western Africa (Haywood et al., 2005). This discrepancy could be reconciled by including mineral dust in the model. The GERBILS experiment, whose full rationale and operating details are described in Haywood et al. (2011), was therefore designed to test this hypothesis, and to determine the properties of the mineral dust to be included in the model. The experiment consisted in ten research flights onboard the FAAM BAe-146 performed between Nouakchott (18.10° N, 15.94° W, Mauritania) and Niamey (13.48° N, 2.18° E, Niger) on an almost standard route along the 18° N meridian. Flights were performed between 18 and 29 June 2007, in a period characterised by a persistent and widespread dust load.

Finally, the Dust Outflow and Deposition to the Ocean (DODO) airborne experiment took place at two different periods in 2006: in wintertime (7–16 February) and in summertime (22–28 August). The aim of DODO was to characterised dust as a possible nutrient for the marine ecosystems. For this reason, the FAAM BAe-146 aircraft was based in Dakar, in Senegal, and most of the twelve research flights (six in the winter period and six in the summer period, respectively) were conducted over the Atlantic Ocean in the outflow from the African continent. However, two flights, one per season, were performed inland above Mauritania in order to sample dust at or very close after emission (McConnell et al., 2008).

Mapping the physico-chemical properties of mineral dust

P. Formenti et al.

Title Page

Abstract

Introduction

Conclusions

References

Tables

Figures

⏪

⏩

◀

▶

Back

Close

Full Screen / Esc

Printer-friendly Version

Interactive Discussion



2.2 Sample collection and handling

2.2.1 Ground-based

Aerosol sampling at the ground-based AMMA super site of Banizoumbou was performed using two identical purpose-built wind-oriented inlets designed for the AMMA field campaigns (Rajot et al., 2008). The cut-off diameter 50 % efficiency of these inlets has been calculated to be approximately 40 μm by using the standard formulae of particle losses in inlets and tubings reported in Baron and Willeke (2001) and Hinds (1999). Each inlet leads to a sampling chamber containing seven different sampling lines, each of them dedicated to a different instrument. Multiple sampling lines are very convenient as they allow collecting various filter samples in parallel, differentiated and optimized in terms of sampling medium, exposure interval and flow rate as a function of the analytical technique to be applied. This also results in minimal manipulation of the filters after sampling. Samples were collected on acid washed 42 mm polycarbonate Nuclepore filters (0.4 μm pore size) mounted on plastic rings. Samples were stored in Petri dishes after sampling. Sampling time was of the order of hours, and was varied depending on the aerosol mass concentration measured on-line by a Tapered Element Oscillating Microbalance (TEOM, Rupprecht and Patashnick, Albany, USA) (Rajot et al., 2008).

2.2.2 Airborne

During the AMMA SOP0-DABEX, DODO and GERBILS campaigns, samples were collected onboard the FAAM BAe-146 aircraft. The aircraft is capable of carrying 2 crew, 18 scientists and a total scientific payload of up to 4000 kg for a distance of 3700 km with a ceiling of 35 000 feet and has a typical science speed of 110 m s^{-1} . For the typical scientific payload, flight patterns, ambient meteorological conditions and the proximity of diversion airports encountered during the campaigns, the average endurance of the BAe146 aircraft was approximately 5 h. Sampling was been performed using a set of two parallel thin-walled inlet nozzles with a curved leading edge; the design was based

Mapping the physico-chemical properties of mineral dust

P. Formenti et al.

Title Page

Abstract

Introduction

Conclusions

References

Tables

Figures



Back

Close

Full Screen / Esc

Printer-friendly Version

Interactive Discussion

Mapping the physico-chemical properties of mineral dust

P. Formenti et al.

[Title Page](#)[Abstract](#)[Introduction](#)[Conclusions](#)[References](#)[Tables](#)[Figures](#)[⏪](#)[⏩](#)[⏴](#)[⏵](#)[Back](#)[Close](#)[Full Screen / Esc](#)[Printer-friendly Version](#)[Interactive Discussion](#)

on criteria for aircraft engine intakes at low Mach numbers (Andreae et al., 1988). The sampling system was operated at flow rates that averaged at 120 L min^{-1} (at ambient pressure and temperature) the flow was adjusted to maintain slightly subsokinetic sampling conditions. The passing efficiency of the inlets has not been formally quantified. During AMMA SOP-0/DABEX, Chou et al. (2008) showed that the number size distributions of the aerosols collected on the filters (counted by electron microscopy) extended up to $10 \mu\text{m}$ diameters and were of comparable magnitude to those measured by wing-mounted optical counters.

Aerosol particles were sampled by filtration onto two stacked-filter units (SFUs) mounted in parallel. Each SFU can hold a maximum of three filters on sequential 47 or 90 mm diameter polyethylene supports. Only one stage was used during the campaigns, i.e., samples represented the aerosol bulk composition. Samples were collected only during horizontal flight legs lasting not less than 20 min in order to guarantee sufficient loading of the filter samples. As a consequence, at the aircraft cruise speed, each sample had at best a spatial resolution of 180 km. Each SFU consisted of a Nuclepore filter (Whatman) of nominal pore size $0.4 \mu\text{m}$.

During the AMMA SOP1-2 campaigns, samples have been collected onboard the SAFIRE ATR-42. With the necessary payload for the campaign, the aircraft had a maximum endurance of 4 h. Minimum flight altitude is 300 m over land. Ceiling is approximately 7 km. The aircraft was equipped with basic sensors for measuring the radiative, dynamic and thermodynamic properties of the atmosphere (Saïd et al., 2010).

Aerosol sampling was performed using the AVIRAD aerosol sampling system newly developed for AMMA (Formenti et al., 2011b). It consists of an iso-axial and isokinetic inlet whose 50% passing efficiency has been estimated at $9 \mu\text{m}$ in diameter. At the cruise speed of the ATR-42 (93 ms^{-1}) the delivered volumetric flow rate is 350 L min^{-1} , which was distributed to various instruments, including two SFU for collecting bulk aerosol samples. Samples were obtained by parallel filtration onto 42 mm diameter polycarbonate membranes (nominal pore size $0.4 \mu\text{m}$ Nucleopore, Whatman) on polyethylene supports. Samples were collected only during horizontal flight legs last-

ing not less than 20 min. Immediately after each flight, the loaded filters were stored in Petri dishes.

Ground-based operation with multiple sampling lines allowed for parallel sampling where the sampling duration is adapted to the characteristics (detection limit, saturation level) of the technique to be employed for analysis. On aircraft, the two parallel samples available had to be manipulated further to allow accommodating the number of analysis one wanted to perform, also taking into account the fact that some analyses are destructive of the sample. Therefore, the handling protocol for aircraft samples consisted in analysing entire filters or portions of those depending on their load on mineral dust. A dedicated tool in polyethylene has been developed for cutting the 47 or 90 mm filters into halves, quarters or eighth without touching and therefore contaminating them.

2.3 Sample analysis

2.3.1 Elemental composition

The total elemental concentrations for elements from Na to Pb by wavelength dispersive X-ray fluorescence (WD-XRF) for samples collected on the ground and on the ATR-42 and Particle-Induced X-ray Emission (PIXE) for the aircraft samples collected onboard the BAe-146. The reason for using different techniques for ground-based and aircraft samples lays on the fact that the WD-XRF sample holder set up could not, at the time, host filters which are not supported on polyethylene frames. The details of the analytical protocols are provided in Formenti et al. (2008, 2011b), McConnell et al. (2008), Rajot et al. (2008) and Klaver et al. (2011). Elemental concentrations are estimated with a 5 % error. An inter-comparison exercise on samples generated in the laboratory from geo-standards of known and certified composition has shown that the two techniques yield comparable results within the error bars (Formenti et al., 2010).

Mapping the physico-chemical properties of mineral dust

P. Formenti et al.

Title Page

Abstract

Introduction

Conclusions

References

Tables

Figures

⏪

⏩

◀

▶

Back

Close

Full Screen / Esc

Printer-friendly Version

Interactive Discussion



2.3.2 Mineralogical composition

The identification of major minerals composing mineral dust: quartz (SiO_2), calcite (CaCO_3), dolomite ($\text{CaMg}(\text{CO}_3)_2$), gypsum ($\text{CaSO}_4 \cdot 2\text{H}_2\text{O}$), clays (kaolinite, illite, smectite, chlorite), feldspars (orthose KAlSi_3O_8 and albite $\text{NaAlSi}_3\text{O}_8$) was performed by X-ray diffraction (XRD) analysis at the Institut de Recherche pour le Développement (IRD) in Bondy, France. The diffractometer, a Siemens D500 with Ni-filtered $\text{Cu-K}\alpha$ radiation, was operated at 40 kV and 30 mA. Samples were scanned from 2 to 70° (2θ) with counting for 10 s every 0.02° (2θ). The analytical procedure and semi-quantitative treatment are fully described by Caquineau et al. (1997), who adapted the sample preparation to low-mass mineral aerosol (load deposited on filter $> 800 \mu\text{g}$). The calibration protocol that was applied to the XRD spectrometer in order to quantify the mineralogical composition is described in Klaver et al. (2011). An improvement of the calibration curves was performed after publication of the Klaver et al. (2011) paper by achieving the calibration for the feldspars (orthose and albite). The calibration factors K_i representing the ratio between the peak surface area S_i in the diffraction spectra and the mass m_i of the i mineral are reported in Table 1. The error on the mineral masses is estimated as the sum of the relative error on the peak area in the diffractograms and on the calibration factor K_i as $\frac{\Delta m_i}{m_i} = \frac{\Delta K_i}{K_i} + \frac{\Delta S_i}{S_i}$. The term $\Delta K_i/K_i$ is estimated from the error of the slope of the calibration curve (Table 1) and it varies between 2 and 10%. The term $\Delta S_i/S_i$ depends on the abundance of the mineral in the samples and has been estimated from the obtained counting statistics.

2.3.3 Iron oxide content and speciation

The iron oxide content, defined as the fraction of iron which is not in the crystal lattice of silicates (Karickhoff and Bailey, 1973), was determined with the adapted Citrate-Bicarbonate-Dithionite (CBD) extraction method developed by Lafon et al. (2004). This method is an adaptation for aerosol filters (with typical material mass less than $500 \mu\text{g}$) of the classical method of (Mehra and Jackson, 1960) for soil analysis. The method

Mapping the physico-chemical properties of mineral dust

P. Formenti et al.

Title Page

Abstract

Introduction

Conclusions

References

Tables

Figures



Back

Close

Full Screen / Esc

Printer-friendly Version

Interactive Discussion



Mapping the physico-chemical properties of mineral dust

P. Formenti et al.

Title Page

Abstract

Introduction

Conclusions

References

Tables

Figures



Back

Close

Full Screen / Esc

Printer-friendly Version

Interactive Discussion

uses a reagent to dissolve iron oxides selectively via reduction. Details of this analysis are given in Formenti et al. (2008, 2011b) and Klaver et al. (2011). The percent error on the iron oxide content is estimated to be 10 % as its assessment is based on two XRF analysis (prior and after dissolution of the iron oxides from the sample).

The speciation of iron oxides was performed by X-ray absorption (XAS) at the Fe K-range: XANES (X-ray Absorption Near Edge Structure) and EXAFS (Extended X-ray Absorption Fine Structure) at the SAMBA (Spectroscopies Applied to Materials based on Absorption, <http://www.synchrotron-soleil.fr/portal/page/portal/Recherche/LignesLumiere/SAMBA>) line SOLEIL synchrotron facility in Saclay, France. XAS spectroscopy is based on the analysis of the position and shape of the K-pre-edge and edge peaks, depending on the oxidation state of iron but also to the atomic position of the neighbouring atoms, mostly O^+ and OH^- . The quantification of the Fe-status was based on the analysis of five standards of Fe(III)-bearing minerals which can be found in mineral dust. Full details of the experimental protocols and the data analysis are provided in Formenti et al., *Dominance of goethite over hematite in iron oxides of mineral dust from western Africa: quantitative partitioning by X-ray Absorption Spectroscopy, submitted to J. Geophys. Res., 2014* (hereafter referred as Formenti et al., 2014).

2.4 Data interpretation and presentation

2.4.1 Source identification

The identification of source regions has been performed using a variety of ancillary products:

1. The record of measurements of the horizontal movement of sand grains by a saltiphone (Eijkelkamp, Giesbeek, the Netherlands) located at the proximity of the sampling inlets at the super-site of Banizoumbou providing with the estimate of the saltation horizontal flux related to established local erosion (Sow et al., 2009).

Mapping the physico-chemical properties of mineral dust

P. Formenti et al.

Title Page

Abstract

Introduction

Conclusions

References

Tables

Figures

⏪

⏩

◀

▶

Back

Close

Full Screen / Esc

Printer-friendly Version

Interactive Discussion

2. Various satellite products, in particular, the daily images of the UV aerosol index by the Ozone Monitoring Instrument (OMI) on Aura; the instantaneous dust product maps from the SEVIRI satellite; and the Infrared Difference Dust Index (IDDI) obtained from the infrared channel of Meteosat (10.5–12.5 μm) (Legrand et al., 1994).

3. Back-trajectories and air mass dispersion calculations using the Met Office Numerical Atmospheric-dispersion Modeling Environment (NAME, Cullen, 1993) and the NOAA HYbrid Single-Particle Lagrangian Integrated Trajectory Model (HYSPLIT) as described in Chou et al. (2008), Rajot et al. (2008) and Klaver et al. (2011).

2.4.2 Data presentation

Calculation of the total mass

In the following, the composition of mineral dust will be presented as percent of the total dust mass (TDM). According to Pye (1987), the TDM can be decomposed as

$$15 \quad \text{TDM} = m_{\text{clays}} + m_{\text{quartz}} + m_{\text{Ca-rich}} + m_{\text{feldspars}} + m_{\text{iron oxides}} + m_{\text{tit oxides}} + m_{\text{organic}} \quad (1)$$

where

m_{clays} = mass of the major clay-species (kaolinite, illite, smectite, chlorite)

m_{quartz} = mass due to quartz (SiO₂)

$m_{\text{Ca-rich}} = m_{\text{calc}} + m_{\text{dolom}} + m_{\text{gypsum}} =$ mass due to calcium carbonates and sulphates

20 in the form of calcite (CaCO₃), dolomite (CaMg(CO₃)₂) and gypsum (CaSO₄)

$m_{\text{feldspars}}$ = mass due to feldspars, such as albite and orthose (NaAlSi₃O₈ and KAlSi₃O₈, respectively)

$m_{\text{iron oxides}}$ = mass due to hematite (α-Fe₂O₃) and goethite (α-FeOOH)

$m_{\text{tit oxides}}$ = mass due to titanium oxides (TiO_2)

m_{organic} = mass due to organic matter which is present in the soils as biological debris and complex organic molecules (humus).

5 In practical terms, the TDM can be approximated by the TEDM (total estimated dust mass) as the sum of the oxide-equivalent of the elemental concentrations of the major elements in mineral dust (Al, Si, Fe, Ca, K, Ti accounted as Al_2O_3 , SiO_2 , Fe_2O_3 , CaCO_3 , K_2O and Ti_2O) whose masses are measured by XRF analysis. The TEDM estimated this way can be compared to the direct measurement of the total dry gravimetric
10 mass (TDGM), which is available for some of the datasets (ground-based AMMA SOP0 and SOP1-2, and GERBILS), either by weighing or by on-line Tapering Element Oscillating Microbalance (TEOM, model 1400a, Rupprecht and Patashnick Albany, New York USA) (see Rajot et al., 2008, and Klaver et al., 2011).

15 The slope of the least-squared linear regression between the TEDM and TDGM, calculated on the 81 samples on which the extraction of iron oxides was performed (see Sect. 3.3), is 0.98 and the coefficient of determination (R^2) is 0.88. This is shown in Fig. 1.

20 This is very satisfactory, taking into account that, because the mass is dominated by coarse particles, which have large mass but little number, differences might arise by losses of some coarse particles between the time at which the filter was weighed and the time at which it was analysed by XRF or by small differences between the filter sampling duration and the TEOM integration times. As a matter of fact, the most of the scatter in the data is observed for samples which corresponded to local erosion or transported emission by convective systems, having the largest fraction of coarse
25 particles and the shortest integration times. This becomes apparent when plotting separately the ground-based AMMA SOP0 and SOP1-2 data (not shown).

Therefore, we consider that the TDM is equal to the TDGM for samples for which the TDGM is measured. When this is not available, the TDM is approximated via the TEDM calculated as sum of oxides. The percent uncertainty is calculated as the squared sum

Mapping the physico-chemical properties of mineral dust

P. Formenti et al.

Title Page

Abstract

Introduction

Conclusions

References

Tables

Figures

◀

▶

◀

▶

Back

Close

Full Screen / Esc

Printer-friendly Version

Interactive Discussion



of the errors on the calculation of the TEDM from the measured Al, Si, Fe, Ca, K, and Ti elemental masses. By doing so, the percent uncertainty on the TDM is 12%.

Calculation of the mineralogical composition

The mass apportionment presented in Eq. (1) has been performed as follows:

1. The masses of quartz, calcite, dolomite, gypsum and feldspar (m_{quartz} , $m_{\text{Ca-rich}}$, $m_{\text{feldspars}}$) are quantified by XRD using the mass/intensity calibration curves as described in Sect. 2.3.
2. The mass of iron oxides ($m_{\text{iron oxides}}$) is measured directly by CBD analysis. The apportionment of $m_{\text{iron oxides}}$ into its main components (hematite and goethite) is performed by XANES spectroscopy.
3. The mass of the clay species, kaolinite, illite, smectite, chlorite (m_{clays}) is estimated by the difference between the TDM and sum of the masses of m_{quartz} , $m_{\text{Ca-rich}}$, $m_{\text{feldspars}}$ and $m_{\text{iron oxides}}$. The apportionment of m_{clays} into its constituting species is difficult to achieve without a direct calibration. This is highly uncertain as there is basically no mineralogical reference having the same crystallographic and chemical status than in the actual aerosol samples, because of the exposure to the environment, weathering in particular, that they experience before and after become airborne. Furthermore, smectite clays are actually a family of species with different chemical characteristics (see the general chemical formulae in Appendix 1 for montmorillonite and nontronite). When only illite and kaolinite are present in the samples, and no traces of chlorite or smectite are shown by XRD analysis, their mass can be apportioned readily using the illite-to-kaolinite ratios (I/K) established by Caquineau et al. (2002) as a function of dust source region as

$$m_{\text{kaolinite}} = \frac{m_{\text{clays}}}{1 + \frac{1}{K}} \quad (2)$$

Mapping the physico-chemical properties of mineral dust

P. Formenti et al.

Title Page

Abstract

Introduction

Conclusions

References

Tables

Figures

⏪

⏩

◀

▶

Back

Close

Full Screen / Esc

Printer-friendly Version

Interactive Discussion



$$m_{\text{illite}} = m_{\text{clays}} - m_{\text{kaolinite}}$$

When smectites or chlorite is also detected, Eq. (3) does not hold true. We will evaluate in the following sections the uncertainties induced by this approximation.

4. The mass of titanium oxides $m_{\text{tit oxides}}$ is estimated by calculating the TiO_2 contribution as the measured elemental Ti multiplied by 1.67, the ratio between the atomic weight of TiO_2 and that of elemental Ti.
5. The mass of organic compounds (m_{organic}) in mineral dust was generally neglected on the basis of the work by Lepple and Brine (1976), it should not exceed 3% of the TDM.
6. We also did not take into account the mass of diatomite fragments which have been observed in samples originated from Bodélé (Chou et al., 2008). Diatomite fragments are silicate skeletons of algae and they do not have a crystalline structure which can be quantified by XRD analysis. Their presence can be put into evidence by elemental analysis as excessive values of the Si-to-Al ratio, up to 4 (Formenti et al., 2011b). The diatomite mass can therefore be estimated by comparing the excess- SiO_2 mass calculated from elemental Si concentrations with respect to the mean ratio-to-Al to the mass of quartz estimated by XRD analysis. When doing so, the excess- SiO_2 mass is comparable to that of quartz except for the few samples for which dust originated from the Bodélé depression in which case their contribution to the TDGM is in the range 6–13%. This contribution is accounted in the error bars of the clay fraction for these samples.

3 Results

The whole dataset (ground-based and airborne AMMA SOP0 and AMMA SOP1-2, GERBILS and DODO campaigns) consists in 704 samples for which we measured

Mapping the physico-chemical properties of mineral dust

P. Formenti et al.

Title Page

Abstract

Introduction

Conclusions

References

Tables

Figures

⏪

⏩

◀

▶

Back

Close

Full Screen / Esc

Printer-friendly Version

Interactive Discussion



Mapping the physico-chemical properties of mineral dust

P. Formenti et al.

Title Page

Abstract

Introduction

Conclusions

References

Tables

Figures



Back

Close

Full Screen / Esc

Printer-friendly Version

Interactive Discussion

the total elemental composition. Out of those, 54 samples have been selected to yield data on the major mineral composition, 86 have been analyzed to yield the content of iron oxide, 12 to determine the iron oxide speciation. 31 samples combined sufficient information to determine the full mineralogical composition. The sample selection has been based on the filter loading and on the possibility of identifying their provenance and attributing them a source region.

3.1 Identification of source regions

The identification of the origin of the mineral dust collected on the samples implies being able to make the link between the knowledge on the position and the mineralogy of the source regions to that of the aerosol samples. To do so, one should know (1) the transfer function, at emission, linking the soil mineralogical/chemical composition to that of the aerosols, and (2) the transfer function describing how its composition is modified during transport.

The first transfer function describes the mineralogical fractionation that occurs between the soil and the aerosol as a consequence of the size segregation happening when the soil grains blast on the soil after saltation (Rahn, 1976). The fractionation can alter the elemental ratio between Si and Al, as a result of the depletion in quartz and feldspars with respect to clays at emission. Quartz and feldspars have higher Si content than clays and are more abundant in the sand than in the silt/clay fractions of the soil (Mason, 1966; Rahn, 1976; Chatenet et al., 1996). These last are enhanced during emission by the saltation/sandblasting (Alfaro et al., 1998). Whereas there is still no systematic assessment of the transfer function between the soil and the aerosol composition, Claquin et al. (1999) have shown that some mass ratios between minerals (for examples, that of illite to kaolinite and that of calcite to quartz) are conserved from the soil to the aerosol if the comparison is restricted to roughly the same size fractions (clays or silt). Lafon et al. (2006) also suggested that the free-iron fraction to the total is conserved.

Mapping the physico-chemical properties of mineral dust

P. Formenti et al.

[Title Page](#)[Abstract](#)[Introduction](#)[Conclusions](#)[References](#)[Tables](#)[Figures](#)[Back](#)[Close](#)[Full Screen / Esc](#)[Printer-friendly Version](#)[Interactive Discussion](#)

The second transfer function describes how the dust composition is modified during transport. Our dataset consists in data which have been collected at most 2 days after emission. We expect that only losses of particles of diameter larger than 10 μm would occur in this short time scale (Pye, 1987). We therefore assume that the chemical/mineralogical composition of our dust aerosol samples is linkable to that of the parent source regions.

To identify the pathway of air masses during transport, and trace them back to an active dust source, we used back-trajectory and dispersion modelling and various satellite products (e.g., Chou et al., 2008; Klaver et al., 2011). This approach does not apply to samples collected in the boundary layer during the Monsoon season south of the Inter-Tropical Convergence Zone (ITCZ). In this case, the dominant flow is from the southwest: dust is present in the boundary layer only as a result of erosion by organized convection or under particularly stable conditions, when high temperatures establish and the thermal turbulence in the boundary layer raises its top height at or above the shear level, bringing dust from the free troposphere in the surface level (Flamant et al., 2009; Formenti et al., 2011b).

Even when applicable, this approach has various caveats: first, if their horizontal velocity is high and exceed the local threshold velocity, air masses within the boundary layer might get loaded with dust along their way before reaching the sampling point. This happens for example when emission is induced by large scale frontal systems as the one of 3–7 March 2006 (Tulet et al., 2008). Secondly, ground-based sampling lasts several hours and the direction of air masses might change in between. Finally, aircraft samples integrate over large areas to which different air masses from different source regions might contribute. This problem might be overcome, or at least minimized, by increasing as much as possible the sampling frequency to match the variability of transport. We did that by following the variability of concentrations, in time or space, with ancillary measurements at higher temporal resolution (mass concentration by the TEOM balance, or the scattering coefficient by a TSI nephelometer).

Mapping the physico-chemical properties of mineral dust

P. Formenti et al.

Title Page

Abstract

Introduction

Conclusions

References

Tables

Figures

⏪

⏩

◀

▶

Back

Close

Full Screen / Esc

Printer-friendly Version

Interactive Discussion



In spite of this, we cannot exclude that our samples might represent larger emission areas than single “hot spots” (see for example, Fig. 1 in Klaver et al., 2011). We do not necessary regard this as a problem, as the atmospheric dust load, both at short and large-scale transport, is often due to a variety of sources active at the same time (Glacuum and Prospero, 1980; Reid et al., 2003; Formenti et al., 2003; Schepanski et al., 2007; Laurent et al., 2008; McConnell et al., 2008; Marticorena et al., 2010). Also, this supra-imposition, both in the vertical and in the horizontal, is what is actually seen by spaceborne sensors. The results of this paper might then be used to build a dust composition model on a scale relevant to satellites.

When doing so, we found that samples presented in this paper are representative of major African sources which, according to Formenti et al. (2011) and Scheuven et al. (2013), are indicated as PSA (Potential Source Area) in Fig. 2.

- The PSA2, including arid areas in western Sahara, Mauritania and Morocco, sampled during the DODO and the GERBILS campaigns. With respect to the extent of this source, the northern part is under-represented as it was sampled on one occasion only.
- The PSA3 represents emitting area in northern Mali and southern Algeria. This is largely the dominant source in terms of frequency of sampling. The air masses travelling from PSA3 often show a recirculating pathway over North Niger. By doing so, at times they might pick up dust from the desert areas close to the Air massif, which is not depicted in Fig. 2, before reaching the sampling site. These occurrences, when identified, are labelled as PSA3+NN.
- The PSA4 was sampled on a few occasions during wintertime. As for PSA3, we have the impression that samples originating from PSA4 often are loaded with dust from northern Niger. A few samples seem to be mainly issued from northern Niger excluding the major identified sources, so this source is referenced as North Niger.

- A few samples also represent dust originated from the Bodélé depression (PSA5). In summertime, a mixture of Sudan and Chad sources including Bodélé might have been sampled (Flamant et al., 2009). Finally, a number of episodes of erosive emissions by convection in the Sahel were also sampled and characterised (referenced as Sahel). These occurred both over Mali and over Niger.

The PSA1 source is not represented in this paper as it was not sampled during the field campaigns.

To provide with a first link between geographical origin and chemical composition, we traced the scatterplot of elemental Si/Al vs. Fe/Ca which we color-coded according to the source region according to satellite/back-trajectories/dispersion modelling information. These ratios have been shown previously to be rather robust indicators of the origin of mineral dust at the large scale (Formenti et al., 2011a and references therein). The result is shown in Fig. 3.

There are some clear distinctions which that can be made. Data points having Si/Al > 3 are unambiguously identified as samples from the Bodélé depression, i.e. PSA 5. Their Fe/Ca ratio is about 1. Data point having Fe/Ca > 3 are related to emission from erosive events in the Sahel. There are various sub-ranges in this group: data having Fe/Ca in the range 3–5 correspond to transported dust aerosol from the Sahel, sampled 1–2 days after emission, corresponding to mixed sources, as PSA3 + Sahel. Data having Fe/Ca > 5 correspond to samples collected immediately or at the very early stage after emission by convective events, mostly locally at the ground-based Banizoumbou site (when the Fe/Ca ratio exceeds 10), but occasionally on uplifted dust onboard aircraft.

Data with Si/Al in the range 2.5–2.9 and Fe/Ca in the range 1–3 have their origins mostly at latitudes in the range 16–27° N, i.e. PSA 3. Whereas the variability of the Si/Al ratio is low, that of Fe and Ca can be used to make some distinctions amongst sources. Fe/Ca higher than 1 is measured for data points from northern Mali, Mauritania, Algeria, northern Niger and Libya whereas Fe/Ca < 1 is for dust from western

Mapping the physico-chemical properties of mineral dust

P. Formenti et al.

Title Page

Abstract

Introduction

Conclusions

References

Tables

Figures

⏪

⏩

◀

▶

Back

Close

Full Screen / Esc

Printer-friendly Version

Interactive Discussion



Sahara (PSA 2). For this source, there are two clear outliers corresponding to samples of dust originating from Morocco and showing the lowest Fe/Ca ratio (~ 0.4).

3.2 Mineralogical composition

The investigation of the mineral composition is based on 51 samples, 15 of which collected onboard aircraft. This dataset is diverse and representative of the variability of sources and emission conditions.

The most evident peaks, for all samples, are those of illite, kaolinite and quartz. Less evident, and not ubiquitous, are the peaks corresponding to feldspars (albite and orthoclase), and calcium-rich minerals (calcite, dolomite, gypsum). Feldspars are found in the samples from local erosion and South Algeria/North Niger/Mauritania and western Sahara. This last set might also contain calcium-rich minerals. Smectite clays are detected as a large and rather weak peak at angles comprised between 4° and 7° . This is indicative of the fact that smectites are a family of weathered clays of different chemical composition (e.g., montmorillonite, nontronite), whose crystalline structure can be heavily modified in the environment. Smectite clays were only evident in samples originated from South Algeria/North Niger/Mauritania and western Sahara.

We can obtain the mass fractions of minerals which can be detected by X-ray diffraction by using the calibration factors as described in Sect. 2.3.2. This of course is not equivalent to the mineralogical composition as a significant part of the mass, in particular that due to iron oxides, is not detected by XRD. These mass fractions are displayed in Fig. 4.

Regardless of the origin, clays and quartz account in average for 87 % (± 6) and 10 % (± 6) of the diffracting mass. There is only one clear outlier in an episode of intense local erosion sampled at the Banizoumbou super-site (sample SOP1-8), for which the percent clay fraction is reduced (56 %), and the quartz and feldspars fraction enhanced (41 and 3.3 %, respectively). This is consistent with the fact that at erosion the size distribution shows an enrichment of coarse particles, whose composition should be closer to that of the soil silt fraction (Gillette and Walker, 1977; Chatenet et al., 1996).

Mapping the physico-chemical properties of mineral dust

P. Formenti et al.

Title Page

Abstract

Introduction

Conclusions

References

Tables

Figures



Back

Close

Full Screen / Esc

Printer-friendly Version

Interactive Discussion



The analysis of the XRD spectra also show that kaolinite and illite are very often the only clay species detected. A broad peak corresponding to smectites was detected on samples from Algeria and at times Bodélé, consistently with finding of Moreno et al. (2006). No chlorite has been detected in our samples. As explained in Sect. 2.4.2, the relative proportions (by mass) of illite and kaolinite have been estimated using the origin-dependent ratios established by Caquineau et al. (2002). For the sources considered in this dataset, the illite-to-kaolinite ratios could vary between 0.1 and 2.3. The central and western Saharan sources (PSA2 and PSA3) display the highest values (1.6 to 2.3) for PSA 5, northern Niger and Sahel the lowest values (0.1 to 0.7).

3.3 Iron oxides content and speciation

The quantification of the content of iron in the oxide form (Fe_{ox}), that is free iron which is not in the crystal lattice of aluminosilicates, has been performed on 81 samples of different origins and load (33 out of those have been collected onboard aircraft). In average, Fe_{ox} account for $58 \pm 7\%$ of the mass of elemental Fe. The range of variability is illustrated in Fig. 5.

The lowest values (down to 44 %) are found for samples of dust originating from the PSA4 (Chad/Egypt) area and for a set of samples collected above the PSA2 areas. The highest values (up to 71 %) are obtained for samples of dust emitted by local erosion in the Sahel, including one episode in which uplifted dust has collected onboard aircraft after emission. Other subset of samples, such as those of dust originated from the South Algeria/North of Niger areas, display equivalently high values when during long-range transport, dust from Algeria mixes with locally-produced dust in Niger. It should be noted also that, because of the internal variability of each group, there is no statistically-significant difference between the iron oxide fractions of the total iron for long-range transported dust originated at latitudes north of 16° N. A broad distinction between the Fe_{ox} -to-Fe ratio of Sahelian samples with respect to those of Saharan samples can be made by sorting the data points by their corresponding Fe/Ca ratio. Mineral dust emitted from the Sahel ($\text{Fe}/\text{Ca} > 3$) are characterized by a mean Fe_{ox} -to-

Fe ratio value of 65 % (± 5 %, standard deviation of the mean), whereas episodes of transport from the Sahara ($\text{Fe}/\text{Ca} < 3$) are characterized by a mean ratio of 56 % (± 6 %). No further distinction based on origin is possible in this second group of samples. This is illustrated in Fig. 6.

X-ray absorption spectroscopy on twelve samples of differing origins indicated that goethite is overall the dominant species of iron oxides. Goethite accounts for 48 to 73 % of the iron oxide mass, whereas hematite accounts for 27 to 52 %. These values do not show a clear trend with respect to the sample origin. The relative proportions of iron in the form of hematite and goethite with respect to total iron are shown in Table 2.

3.4 Titanium oxides content

Titanium oxides deserve attention as they are involved in photo-catalytical heterogeneous reactions with various atmospheric constituents, including volatile and semi-volatile organic compounds which are found in transport regions of mineral dust due to biomass burning emissions (Gustafsson et al., 2006).

We therefore examined our dataset in order to provide with estimates of the content of titanium oxides in mineral dust from various sources in western Africa. The titanium oxide content has been estimated from the measured element Ti concentration (obtained by XRF) which is converted to TiO_2 using the appropriate molar mass conversion factor (1.67). This should be considered as an upper limit estimate as some of the titanium in mineral dust is present as substitution element in aluminosilicates, which we have observed at times in individual particles (Chou et al., 2008).

Figure 7 presents the correlation between the TiO_2 and the TDM. Two populations can be identified: one corresponding to samples collected in correspondence of erosion events and one corresponding to advection events. For both populations, the correlation is excellent (R^2 equal to 0.97 and 0.92, respectively) and the scatter of points is minimal. The TiO_2 content is higher in erosion events from the Sahelian region (average 1.2 % (± 0.1) of the mass), than for advection events of Saharan dust, for which TiO_2 represents in average 0.71 % (± 0.01) of the mass.

Mapping the physico-chemical properties of mineral dust

P. Formenti et al.

Title Page

Abstract

Introduction

Conclusions

References

Tables

Figures

⏪

⏩

◀

▶

Back

Close

Full Screen / Esc

Printer-friendly Version

Interactive Discussion



Looking at the elemental ratios between Ti, Fe, and Fe_{ox} provides with further insights (Fig. 8). The ratio of Ti-to-Fe is insensitive to changes in the Fe_{ox} proportions to Fe up to 60 %, and then starts increasing linearly with increasing Fe_{ox}-to-Fe ratio. This suggests that, in Sahelian dust, Ti is associated with iron oxides but not in Saharan dust.

3.5 Mass apportionment of the mineralogical composition

By crossing the information presented in Sect. 3.1 to 3.4, we can estimate the mineralogical composition of samples of mineral dust of local or distant origin.

The mass apportionment is shown in Table 3. Note that we provide here with the composition of the bulk mineral dust, without explicitly taking into account the dependence on size.

There are clear similarities in the composition of the dust from those different origins, first of all in the fact that the clay fraction represents the largest fraction of the dust mass. Also note the absence of Ca-rich minerals (calcite, dolomite, gypsum) in dust originating from the Sahel compared to that originated elsewhere.

Despite the overall similarities, there is indeed a large internal variability within each source group, expressed by the standard deviation around the mean, and which might be related to either the time or height after transport.

An example can be given by looking at the composition of the four samples in Bodélé/Sudan group: one sample was collected in the dry season, whereas the remaining three are sequenced samples collected in the wet season, at a time characterised by the absence of local emission, but by a progressively increasing entrainment of dust transported from the free troposphere to the surface layer (J. L. Rajot, personal communication, 2013). These wet-season samples have a lower clay fraction and a higher quartz and feldspar content (in the range 7–18 % and 0.4–0.8, respectively). This variability corresponds to differences in the volume size distribution, normalised to the total volume for sake of comparison (Fig. 9). As a matter of fact, the volume size distribution of the dry-season sample presents a large coarse mode peaking around 4–5 μm,

Mapping the physico-chemical properties of mineral dust

P. Formenti et al.

Title Page

Abstract

Introduction

Conclusions

References

Tables

Figures

⏪

⏩

◀

▶

Back

Close

Full Screen / Esc

Printer-friendly Version

Interactive Discussion



Mapping the physico-chemical properties of mineral dust

P. Formenti et al.

Title Page

Abstract

Introduction

Conclusions

References

Tables

Figures

⏪

⏩

◀

▶

Back

Close

Full Screen / Esc

Printer-friendly Version

Interactive Discussion



5 pended particulate concentrations around $100 \mu\text{g m}^{-3}$) in Morocco. Quartz accounts for as high as $\sim 65\%$ in dust storm conditions, suggesting that soil grains, and not only aerosols, were sampled. Conversely, low-dust conditions are characterised by only about 20 % of quartz. These authors showed that, for locally emitted dust, illite is the dominant clay form over kaolinite (up to 30 and 5 % by volume, respectively). These authors also detected clay in the form of chlorite (less than 10 % by weigh) and calcite (up to 15 %).

10 Few authors have published data on the iron oxide content. Lafon et al. (2004) evaluated the free-to-total iron content in samples collected at the Banizoumbou ground-based site and found mean values of $0.44 (\pm 0.11)$ and $0.65 (\pm 0.04)$ for dust transported in the Harmattan flow (from the Sahara) and dust emitted locally by convective erosion. Lazaro et al. (2008) found sensibly lower values than ours ranging from 0.26 to 0.63 but only exceeding 0.56 in three occasions when back-trajectories indicated transport from the Sahel or a mixture of dust originating from the Sahara and the Sahel. Our values are on the higher side with respect to those of these authors. Nonetheless, the back-trajectories presented in the paper seem indicating that the Saharan dust originated from higher latitudes than the one we sampled – and mostly from Tunisia and Algeria. It will be interesting in the future to sample those source areas to confirm these rather low values.

20 Finally, our results on the iron oxide speciation are consistent with findings of different authors using XANES speciation (Wilke et al., 2001; Ohta et al., 2006; Prietzel et al., 2007; Majestic et al., 2007) and visible spectroscopy (Arimoto et al., 2002) indicating that Fe(III) is the dominant red-ox form of iron oxides and that goethite is the predominant form of iron oxide over hematite.

25 4.2 Atmospheric implications

The results showed in this paper suggest that, when restricted to the mass fraction below $20 \mu\text{m}$, the dust composition in western Africa may apparently be simplified to few

Mapping the physico-chemical properties of mineral dust

P. Formenti et al.

Title Page

Abstract

Introduction

Conclusions

References

Tables

Figures

◀

▶

◀

▶

Back

Close

Full Screen / Esc

Printer-friendly Version

Interactive Discussion



minerals, clays, quartz, calcite, iron and titanium oxides. Feldspars and other calcium-containing minerals such as dolomite and gypsum are very minor components close to detection limits. The geographical distribution of the dust composition is relatively unimportant in terms of mass fractions, in particular in comparison to the importance of the size distribution whose variability with time seems to be able to explain some differences observed between samples from the same source region at different times after emission. Nonetheless, it is important to evaluate whether differences in the composition at the regional scale, even when minor, might give raise to differences in the impacts of mineral dust.

To do so, we explore the influence of dust composition on the spectral complex refractive index \tilde{n} and the fraction iron solubility.

4.2.1 Implications for optical properties

As a mean of evaluating the effect of the variability of the composition on the dust optical properties, the volume-average refractive index has been calculated as

$$\tilde{n} = \sum_j f_j \times \tilde{n}_j \quad (3)$$

where f_j is the volume fraction of each individual mineral in the dust sample (as reported in Table 3) and \tilde{n}_j is its complex refractive index. Equation (3) assumes that minerals in dust are in internal mixing. In reality, minerals are present in dust as external mixtures, with the exception of iron oxides which may be found as inclusions in clays (Sokolik and Toon, 1999). However, the internal mixing hypothesis is frequently used in experiments and climate models (e.g., Balkanski et al., 2007; Kandler et al., 2009; McConnell et al., 2010; Hansell et al., 2011).

Values of the complex refractive index \tilde{n}_j of the individual minerals detected in our samples are listed in Table 4. We have restricted the calculations to two spectral domains: the near UV-visible between 370 and 700 nm and the thermal IR from 8 to 15 μm , where values for all individual minerals are available.

Mapping the physico-chemical properties of mineral dust

P. Formenti et al.

Title Page

Abstract

Introduction

Conclusions

References

Tables

Figures

⏪

⏩

◀

▶

Back

Close

Full Screen / Esc

Printer-friendly Version

Interactive Discussion



Results are presented in Fig. 11, where they are compared to the values of the “desert” dust aerosol model in the OPAC (Optical Properties of Aerosols and Clouds) database (Hess et al., 1998), which is often used in satellite retrieval algorithms in the thermal infrared (see Table 1 in Klüser et al., 2012), but also in radiative transfer calculations (Highwood et al., 2003; Haywood et al., 2005). The “desert” model in the OPAC database represents the properties of mineral dust at source region, considered as a mixture of quartz and clays in different size fractions.

We restrict Fig. 11 to the visible and infrared imaginary parts of the complex refractive index \tilde{n}_i , from which the absorption coefficient σ_a as a function of wavelength λ can be estimated as $4\pi\tilde{n}_i/\lambda$ (Bohren and Huffman, 1987).

In the visible, the imaginary part of the complex refractive index is relatively constant with wavelength. Mean values are of the order of 0.003, with standard deviation of the order of 0.001, with the exception of data from the PSA4 source, which average at 0.006 and present a standard deviation (0.003). It is difficult to judge on this variability as it is induced by one sample only presenting an outstanding iron oxide fraction.

In the infrared, the imaginary part show a band-type structure in correspondence to the major absorption bands of clays and quartz, mostly found in the atmospheric window between 8 and 11 μm . There is very little sample-to-sample variability in the position of the bands, as well as in the relative proportions of the band peaks, with the exception of the Sahelian dust samples, which present a larger standard deviation due to the enhancement of the band at 9.2 μm corresponding to the outstanding quartz fraction of sample SOP1-8. Furthermore, whereas there is very little difference in the spectra of sources PSA3, PSA4 and to a lesser extent PSA5, which have the highest absorption values at 9.6 μm , the spectral dependence for dust from source PSA2 is different (peak at 9.2 μm more pronounced than that at 9.6 μm) because of the higher fraction of illite.

The comparison of the composition-based refractive indices calculated in this work with data of the OPAC database shows some discrepancies.

Mapping the physico-chemical properties of mineral dust

P. Formenti et al.

Title Page

Abstract

Introduction

Conclusions

References

Tables

Figures

⏪

⏩

◀

▶

Back

Close

Full Screen / Esc

Printer-friendly Version

Interactive Discussion

sum of Fe solubility of various minerals compounding iron in the dust matrix. We propose to apply this calculation to this dataset to estimate the solubility of dust in source region. In this purpose, we use the iron solubility from minerals measured by Paris et al. (2011) at pH = 4.7 which a typical pH of African rainwaters (Desboeufs et al., 2010), i.e. SFe equal to 0.17% for illite and 0.006% for free iron from goethite and hematite. Paris et al. (2011) made the approximation that all the iron associated to clay is present as illite. Journet et al. (2008) emphasized that even the iron in impurities into kaolinite or feldspars matrix present a high solubility. Our measurements show the predominance of kaolinite in comparison to illite, so we consider also the dissolution of Fe from kaolinite due to the large proportion of this mineral in the studied samples. We use a SFe = 0.63% for kaolinite (R. Paris, personal communication, 2013). The percent quantity of feldspar being usually inferior to 1% in the samples, we neglect the iron associated to these minerals. Finally, the smectites, such as montmorillonite, are also minerals with high content of iron with a higher solubility (Journet et al., 2008). However, due to the difficulties in quantifying the smectite fraction, this other source of structural Fe is not well constrained.

Among the samples present in our database, the mineralogical composition including goethite, hematite, illite and kaolinite is evaluated for 27 samples, enabling to calculate the iron fractional solubility (Table 3). In this case, the iron content in illite is assumed equal to $4.0 \pm 0.9\%$, which corresponds to the mean stoichiometric value of two types of illites (Fithian, Illinois and Rochester, Minnesota, as shown in Journet et al., 2008). The iron content in illite can vary from 0.8 to 8.4% (Murad and Wagner, 1994), this large range is due to the fact that Fe is present as substitution of Al or K in the sheet-like structure of illite, and this will depend on the environmental conditions that the clay has experienced in the soil fraction (weathering, . . .). In goethite and hematite, we estimated the iron content based on the analysis of Journet et al. (2008) and Paris et al. (2011) as 62.9 and 57.5% for goethite and hematite, respectively. For kaolinite, Mestdagh et al. (1980) show that the iron content is related to the cristallinity of the

mineral and ranges from 0.02 to 0.81 % with an average of $0.4\% \pm 0.2\%$, which is used for our calculation.

In order to have a larger view of the variability of iron solubility as a function of emission source, we can also calculate iron solubility from the partitioning between structural and free iron as obtained by the CBD extraction analysis (Table 2). This is doable for 85 samples, among which the 27 samples for what the mineralogical composition is estimated. In this case, we consider the structural iron ($\%Fe_{\text{structural}}$) is associated to illite ($\%Fe_{\text{illite}}$) and kaolinite ($\%Fe_{\text{kaolinite}}$) in the proportion of illite-to-kaolinite ratio corresponding to the origin of the samples (see Sect. 3.2), such as:

$$\%Fe_{\text{kaolinite}} = \frac{\%Fe_{\text{structural}}}{\left(1 + 10 \times \frac{1}{K}\right)} \quad (4)$$

and

$$\%Fe_{\text{illite}} = \%Fe_{\text{structural}} - \%Fe_{\text{kaolinite}} \quad (5)$$

with 10 represents the illite-to-kaolinite iron content ratio (4.0%/0.4%)

Results are summarized in Fig. 12.

The mean value of iron fractional solubility is 0.10 % ($\pm 0.02\%$) whatever the methods of calculation, i.e. from mineralogical composition or from CBD extraction analysis. There is little variability of iron solubility as a function of the source; nonetheless, this is directly opposite to the iron oxide content, i.e., the lowest values ($0.08\% \pm 0.01\%$) obtained for samples of dust emitted by local erosion in the Sahel, in agreement with the highest iron oxides content. Inversely, the samples with the highest solubility ($0.13\% \pm 0.01\%$) issued from PSA3, i.e. South Algeria/Mali which present a low % of free iron (49%). Data show that 54 to 87 % of soluble iron is structural iron associated to illite, meaning that this mineral is the major provider of soluble iron in our conditions of calculation. The determining factor for this parameter is the quantification of illite and hence the hypothesis made on the illite-to-kaolinite ratio as a function of emission

Mapping the physico-chemical properties of mineral dust

P. Formenti et al.

Title Page

Abstract

Introduction

Conclusions

References

Tables

Figures

⏪

⏩

◀

▶

Back

Close

Full Screen / Esc

Printer-friendly Version

Interactive Discussion



Mapping the physico-chemical properties of mineral dust

P. Formenti et al.

Title Page

Abstract

Introduction

Conclusions

References

Tables

Figures

⏪

⏩

◀

▶

Back

Close

Full Screen / Esc

Printer-friendly Version

Interactive Discussion



source, which is estimated from Caquineau et al. (2002). Thus, the regional variability on iron solubility obtained here is mainly associated with this ratio which should be better constrained. A rapid calculation for the PSA3 samples, the richest in structural iron, show that the iron solubility is divided by a factor 2 when $1/K$ varies from 0.1 to 2.3, the extreme values observed by Caquineau et al. (2002). This means that the solubility between the various emission sources varies at the best by a factor 2. Another source of error could be the estimation of iron oxide which is affected by 30 % errors (and those of illite too, by extension). Sample-to-sample comparison shows that there is a rather good correspondence with the two methods of calculation (within 15%). However, the calculation based on mineralogy yields values lower by a factor of 1.5 for the samples issued from PSA3 alone or in mixing with other sources, meaning an underestimation of structural iron in comparison from the direct measurements by CBD analyses. Smectites are identified for several samples of this source, we underestimate so the calculated solubility for the samples where these minerals are present.

The mean fractional iron solubility obtained by calculation is consistent but rather inferior to the observations obtained for transported Saharan dust over Atlantic which ranges from 0.12 to 4.1 % (Sarhou et al., 2003; Baker et al., 2006; Sholkovitz et al., 2012). However, our calculation are exclusively based on mineralogical parameters, since our samples have been collected at most 2 days after emission and do not integrate the various chemical and physical processes increasing dust solubility during long range transport, as cloud process (Desboeufs et al., 2001); photochemical process (Hand et al., 2004) or organic complexation (Paris et al., 2013). Thus, the range of calculated values could be representative of iron solubility for the various sources of African dust before transport. Moreover, the limited regional variability estimated here in comparison to the variability of measurements over Atlantic Ocean show that the emission source of dust is less critical than the process after transport to estimate the fractional iron solubility of dust. Nevertheless, new direct measurements of the iron fractional solubility for sources of dust in western Africa are necessary to validate these conclusions.

5 Final remarks, conclusions and perspectives

In this paper we have presented an insight on the mineralogical composition of mineral dust from western Africa from the synthesis of the airborne and ground-based observations of field campaigns conducted between 2006 and 2007. These observations have been performed at emission or within 2 days of transport in the atmosphere. The strength of this synthesis resides in the fact that the observations have been performed in a consistent way from the methodological point of view (both for the sample collection and analysis) and that they span a large geographical region covering some of the major African dust sources.

The composition data presented in this paper are being made public on a dataset called DUST-MAP, to date still on its trial version. Meanwhile, data are available upon request. The perspective evolution of this dataset will be the inclusion of data from other field campaigns, both close to source regions than over transport zones. Amongst those are the FENNEC and the SAMUM field campaigns (Heintzenberg et al., 2008; Ansmann et al., 2011; Washington et al., 2012), which were conducted downwind sources in Algeria and Morocco relevant to large-scale transport (Caquineau et al., 2002). This will require a close-up examination of experimental protocols and a careful evaluation of their influence on the results.

The presentation of this work deserves some final considerations and opens various perspectives.

The bulk mineralogical composition of dust in western Africa can be described by a simple model where kaolinite and illite account for 80 % or above of the mass, and quartz, iron and titanium oxides for the remaining 20 %. Calcite is a distinctive element of Saharan sources for which it ranges between 0.3 and 8.4 % in dust mass. For the remaining minerals, the variability is due to source type (e.g., the proportions of illite and kaolinite as evidenced by Caquineau et al., 2002) or to differences in the size distribution, particularly the increase of the quartz fraction corresponding to a coarse mode centred around 8 μm in diameter. For the first time to our best knowledge, we

Mapping the physico-chemical properties of mineral dust

P. Formenti et al.

Title Page

Abstract

Introduction

Conclusions

References

Tables

Figures



Back

Close

Full Screen / Esc

Printer-friendly Version

Interactive Discussion

Mapping the physico-chemical properties of mineral dust

P. Formenti et al.

Title Page

Abstract

Introduction

Conclusions

References

Tables

Figures

⏪

⏩

◀

▶

Back

Close

Full Screen / Esc

Printer-friendly Version

Interactive Discussion



provide with a large dataset of titanium oxide data which can be relevant to atmospheric photochemistry (N'Dour et al., 2009). We estimate that Sahelian dust is composed by 2 % (by mass) of titanium oxides, that is, double the mass fraction of dust from sources in the PSA2, PSA3, PSA4 and PSA5 areas, with very little sample-to-sample variability.

5 Iron oxides, also important for atmospheric chemistry processes and radiation, display higher values in Sahelian than in Saharan dust.

The discussion of the regional variability of the mineralogical composition is based on our ability in detecting source areas based on satellite remote sensing or on soil properties map (e.g., Schepanski et al., 2007; Laurent et al., 2008), and in attributing the provenience of an air mass to it via back-trajectory calculations (e.g., Klaver et al., 10 2011). Beside uncertainties related to the methodology, in particular in the definition of source areas, there will be an inherent ambiguity on source attribution based on the fact that air masses, especially when they travel in the boundary layer (winter-time transport) might uplift dust aerosols at various times during transport (Klaver, 2012), and to the fact that aircraft samples might integrate transport from various sources active at the same time due to the fact that aircraft moves during sampling and that sample collection lasts at least 20 min, corresponding to about 120 km at typical aircraft cruise speed. It is therefore clear that some fine features of the mineralogy specific to individual sources might be lost. Nevertheless, our data well represent the composition of the regional dust load as it results from the natural mixing that occurs in the atmosphere during transport. They are also of comparable spatial resolution to that of various state-of-the-arts global and regional circulation models including dust mineralogy (Balkanski et al., 2007; Hoose et al., 2008; Huneus et al., 2010). Henceforth, the composition data presented in this paper may serve to evaluate the regional and global model estimates of the dust mineralogical composition in the western African atmosphere and to calculate dust properties relevant to their direct, indirect and biogeochemical impacts. Claquin et al. (1999) have discussed some comparisons between the mineralogy of dust atmospheric data and that of the soil fraction predicted by a surface mineralogy table constructed from maps of the arid soil mineralogy (updates of this 20 25

Mapping the physico-chemical properties of mineral dust

P. Formenti et al.

Title Page

Abstract

Introduction

Conclusions

References

Tables

Figures

⏪

⏩

◀

▶

Back

Close

Full Screen / Esc

Printer-friendly Version

Interactive Discussion

table have been recently published by Nickovic et al. (2012) and Journet et al. (2013)). To do so, these authors have calculated weight ratios between some minerals (calcite, feldspar and hematite, where hematite is meant to represent the sum of the content of goethite and hematite) with respect to quartz. Our data are consistent with the Claquin et al. (1999) dataset regarding the variability of the calcite-to-quartz ratio, but display higher and lower ratios for hematite and feldspar, respectively. Our ratio of hematite-to-quartz ranges between 0.03 and 1 (0.09 and 3 when the sum of goethite and hematite is considered) instead than 0.009–0.09, whereas our ratio feldspar-to-quartz is in the range 0.03–0.11 instead that 0.2–2 in Claquin et al. (1999). These differences illustrate the fact that our data are closer to representing the clay soil fraction, whereas the data of Claquin et al. (1999) best represent also the silt fraction, richer in quartz particles. When limited to sample SOP1-8, the local erosion sample enriched in quartz and in the particle fraction larger than 20 μm , ratios are 0.09 for hematite-to-quartz (0.03 if hematite only is considered) and 0.08 for feldspar-to-quartz, in the range expressed by Claquin et al. (1999).

Finally, we have provided with the estimate of parameters which are relevant to the direct impact of mineral dust on radiation and on the ocean productivity: the complex refractive index \tilde{n} and the iron fractional solubility SF_e.

Assuming internal mixing, we have shown that the complex index of refraction based on mineralogy has some variability mostly related to the partitioning between illite and kaolinite and to the quartz fraction when this overcomes 40 % of the dust volume. The spectral behaviour of the estimated complex index of refraction has little correspondence with the model proposed by the OPAC database. The OPAC approach overestimates absorption in the visible. On the other hand, a very recent study presents values of the complex refractive index in the shortwave based on a global mineralogy soil map (Schmid et al., 2013). At 550 nm, these authors predict a real part of the complex refractive index around 1.56, that is, higher than our which ranges between 1.45 and 1.51. Their imaginary part averaging at 6.2×10^{-4} , that is, almost an order of magnitude lower than our predicted values (average 3×10^{-3}). This is the consequence of the fact

Mapping the physico-chemical properties of mineral dust

P. Formenti et al.

Title Page

Abstract

Introduction

Conclusions

References

Tables

Figures

⏪

⏩

◀

▶

Back

Close

Full Screen / Esc

Printer-friendly Version

Interactive Discussion



that optical properties estimated from the soil fraction will reflect more closely the optical properties of quartz, which, is enriched in the soil fraction but which in the aerosol fraction due to the size fractionation at emission. An additional confirmation is given by the fact that, in our data, the highest value of the real part of the complex refractive index is obtained for sample SOP1-8, representing the Sahelian erosion case with the highest quartz fraction (41 % by weight), whereas the highest values of the imaginary part are obtained for samples representing long-range transport from Libya through north Niger, having a low or even the lowest quartz percentage by weight (1.5–6 %) but having the highest calcite fraction (4–8 % by weight). As a matter of fact, quartz is transparent in the visible, whereas calcite, but also clays are absorbing. These considerations bring to the conclusion that not only the soil mineralogy but also the transfer function between the soil and the aerosol fractions must be implemented in models estimating the dust optical properties.

In the longwave spectrum, our calculations suggest higher absorption than the OPAC model in the atmospheric window. The 10–12 μm band, which is sensitive to differences in the mineralogical composition amongst sources, is relevant to the retrieval of various space-borne sensors, including IASI, AIRS, and MODIS (De Souza Machado et al., 2006; Hudson et al., 2008; Klüser et al., 2011; Laskina et al., 2012). We expect differences between our values and the OPAC database to be, at least partially, due to differences in the optical constants of the individual minerals. Dedicated in situ measurements of the optical constants of the dust samples would allow confirming this hypothesis and helping understanding the differences.

Nonetheless, a limitation of this work, impacting the refinement of the estimate of the complex refractive index, is the quantification of smectite-type clays. For the purposes of the present study, we have chosen to neglect the contribution of smectites, which were detected only on a few samples, and which we consider as a trace component of the aerosol. Also, smectites are dominant in the 0.2 μm size fraction, which is poor in mineral dust in our samples (Klaver, 2012).

Mapping the physico-chemical properties of mineral dust

P. Formenti et al.

Title Page

Abstract

Introduction

Conclusions

References

Tables

Figures

⏪

⏩

◀

▶

Back

Close

Full Screen / Esc

Printer-friendly Version

Interactive Discussion

In the visible Egan and Hilgeman (1979) indicated that two different montmorillonite types (one from Wyoming and one from Mississippi) have refractive indices very close, both in spectral dependence and magnitude, either to those of kaolinite or illite, respectively, although below 500 nm the imaginary part of the complex refractive index of the montmorillonite from Mississippi is higher by a factor of 2 than that of illite, reaching 0.004 between 200 and 360 nm. In the infrared, various authors (Toon et al., 1976; Glotch et al., 2007; Hudson et al., 2008) have shown that montmorillonite has similar optical properties to those of illite, albeit displaying higher intensity of extinction around 9.5 μm , in the Si–O stretching band. Köster et al. (1999) examined 5 types of nontronites and Fe-rich smectites and found that the position and the intensity of this band vary depending on tetrahedral Fe(III) content. Also, the speciation of clays, in particular that of montmorillonite, has implications for the cloud and ice nucleation properties of mineral dust and the estimate of iron fractional solubility (Hoose et al., 2008; Journet et al., 2008). Ultimately, these facts depend on the compositional heterogeneity in Al-rich smectite in the natural soils and sediments (Christidis and Dunham, 1993, 1997; Christidis, 2006), due to various processes, including weathering and/or hydrothermal alteration of basic rocks (Köster et al., 1999), but also reduction reactions of structural Fe by microorganisms (Pentrakova et al., 2013). This makes their quantification extremely dependent on the environmental conditions. Similar considerations will hold for chlorite-type clays, which were not detected in our samples, but might be present in dust from North African deserts such as Morocco and Tunisia (Paquet et al., 1984; Kandler et al., 2009). It should be noted that to date no measurements of the complex refractive index of chlorites are available in the shortwave. In the longwave, chlorite has significantly different optical properties than illite and kaolinite, in particular concerning their major absorption bands, which is located at 9.6 μm for illite and kaolinite, and at 10.2 μm for chlorite (Egan and Hilgeman, 1979; Mooney and Knacke, 1985). Should chlorite be detected in the samples, its lack of quantification will be treated as an additional source of error to be evaluated.

Mapping the physico-chemical properties of mineral dust

P. Formenti et al.

Title Page

Abstract

Introduction

Conclusions

References

Tables

Figures



Back

Close

Full Screen / Esc

Printer-friendly Version

Interactive Discussion

Regarding the iron fractional solubility, we estimate that the SFe in source regions (0.1 %) is in the lowest range of measurements for dust collected over the Atlantic Ocean, confirming an effect of transport on the value of solubility. The determining parameter to explain for the calculation of iron solubility is the illite-to-kaolinite ratio since illite is the major provider of soluble iron. However, this ratio is estimated from one set of measurements (Caquineau et al., 2002) and should be better constrained. Our data are not conclusive in identifying a clear difference with respect to the source region in comparison to the variability observed on dust collected over the Atlantic Ocean. Thus, this limited regional variability suggest the relevance to use one value of reference for the fractional solubility of Saharan and Sahelian dust before atmospheric long-range transport in biogeochemical models. However, this implies also the need to consider atmospheric processes to reproduce the range of iron solubility observed over Atlantic Ocean. Nonetheless, our calculated values need to be confirmed by field measurements in emission sources, which are unavailable for the moment.

Acknowledgements. This research was funded by several institutions. Based on a French initiative, AMMA was built by an international scientific group and is currently funded by a large number of agencies, especially from France, the UK, the United States, and Africa. It has been the beneficiary of a major financial contribution from the European Community's Sixth Framework Research Programme. Detailed information on scientific coordination and funding is available on the AMMA International Web site at www.amma-international.org. Financial support by the API-AMMA and LEFE (project BIRD) French national funding programs is also acknowledged. The participation of P. Formenti to the DODO and GERBILS field campaigns was supported and by the UK NERC and by the UK MetOffice, which are gratefully acknowledged.

Thanks are also due to the LISA personnel who participated in field campaigns and helped with sample collection, as well as to the BAe-146 and SAFIRE air and ground crews, as well as the FAAM and Met Office observers.

References

- Abdourhamane Toure, A., Rajot, J. L., Garba, Z., Marticorena, B., Petit, C., and Sebag, D.: Impact of very low crop residues cover on wind erosion in the Sahel, *Catena*, 85, 205–214, doi:10.1016/j.catena.2011.01.002, 2011.
- 5 Alfaro, S. C., Gaudichet, A., Gomes, L., and Maillé, M.: Mineral aerosol production by wind erosion: aerosol particle sizes and binding energies, *Geophys. Res. Lett.*, 25, 991–994, 1998.
- Andreae, M. O., Berresheim, H., Andreae, T. W., Kritz, M. A., Bates, T. S., and Merrill, J. T.: Vertical distribution of dimethylsulfide, sulfur dioxide, aerosol ions, and radon over the Northeast Pacific ocean, *J. Atmos. Chem.*, 6, 149–173, 1988.
- 10 Ansmann, A., Petzold, A., Kandler, K., Tegen, I. N. A., Wendisch, M., Müller, D., Weinzierl, B., Müller, T., and Heintzenberg, J.: Saharan Mineral Dust Experiments SAMUM-1 and SAMUM-2: what have we learned?, *Tellus B*, 63, 403–429, doi:10.1111/j.1600-0889.2011.00555.x, 2011.
- Arimoto, R., Balsam, W., and Schloesslin, C.: Visible spectroscopy of aerosol particles collected on filters: iron-oxide minerals, *Atmos. Environ.*, 36, 89–96, 2002.
- 15 Atkinson, J. D., Murray, B. J., Woodhouse, M. T., Whale, T. F., Baustian, K. J., Carslaw, K. S., Dobbie, S., O'Sullivan, D., and Malkin, T. L.: The importance of feldspar for ice nucleation by mineral dust in mixed-phase clouds, *Nature*, 498, 355–358, doi:10.1038/nature12278, 2013.
- Balkanski, Y., Schulz, M., Claquin, T., and Guibert, S.: Reevaluation of Mineral aerosol radiative forcings suggests a better agreement with satellite and AERONET data, *Atmos. Chem. Phys.*, 7, 81–95, doi:10.5194/acp-7-81-2007, 2007.
- 20 Baron, P. A. and Willeke, K.: *Aerosol Measurement: Principles, Techniques and Applications*, 2nd edn., John Wiley and Sons, New York, 2001.
- Barthelmy, D.: Mineralogy database, available at <http://www.webmineral.com> (last access: 1 September 2013), 2007.
- 25 Bedidi, A. and Cervelle, B.: Light scattering by spherical particles with hematite and goethite like optical properties: effect of water impregnation, *J. Geophys. Res.*, 98, 11941–11952, 1993.
- Ben-Ami, Y., Koren, I., and Altaratz, O.: Patterns of North African dust transport over the Atlantic: winter vs. summer, based on CALIPSO first year data, *Atmos. Chem. Phys.*, 9, 7867–7875, doi:10.5194/acp-9-7867-2009, 2009.
- 30

Mapping the physico-chemical properties of mineral dust

P. Formenti et al.

Title Page

Abstract

Introduction

Conclusions

References

Tables

Figures

⏪

⏩

◀

▶

Back

Close

Full Screen / Esc

Printer-friendly Version

Interactive Discussion



**Mapping the
physico-chemical
properties of mineral
dust**

P. Formenti et al.

Title Page

Abstract

Introduction

Conclusions

References

Tables

Figures

◀

▶

◀

▶

Back

Close

Full Screen / Esc

Printer-friendly Version

Interactive Discussion



Ben-Ami, Y., Koren, I., Rudich, Y., Artaxo, P., Martin, S. T., and Andreae, M. O.: Transport of North African dust from the Bodélé depression to the Amazon Basin: a case study, *Atmos. Chem. Phys.*, 10, 7533–7544, doi:10.5194/acp-10-7533-2010, 2010.

Bristow, C. S., Drake, N., and Armitage, S.: Deflation in the dustiest place on Earth: the Bodélé Depression, Chad, *Geomorphology*, 105, 50–58, doi:10.1016/j.geomorph.2007.12.014, 2009.

Brooks, N. and Legrand, M.: Dust variability over North Africa and rainfall in the Sahel, in: *Linking Climate Change to Land Surface Change, Advances in Global Change Research*, Kluwer Academic Publishers, Dordrecht, 1–25, 2003.

Caquineau, S., Magonthier, M.-C., Gaudichet, A., and Gomes, L.: An improved procedure for the X-ray diffraction analysis of low-mass atmospheric dust samples, *Eur. J. Mineral.*, 9, 157–166, 1997.

Caquineau, S., Gaudichet, A., Gomes, L., and Legrand, M.: Mineralogy of Saharan dust transported over northwestern tropical Atlantic Ocean in relation to source regions, *J. Geophys. Res.*, 107, 4251, doi:10.1029/2000jd000247, 2002.

Carlsaw, K. S., Boucher, O., Spracklen, D. V., Mann, G. W., Rae, J. G. L., Woodward, S., and Kulmala, M.: A review of natural aerosol interactions and feedbacks within the Earth system, *Atmos. Chem. Phys.*, 10, 1701–1737, doi:10.5194/acp-10-1701-2010, 2010.

Chatenet, B., Marticorena, B., Gomes, L., and Bergametti, G.: Assessing the microped size distributions of desert soils erodible by wind, *Sedimentology*, 43, 901–911, doi:10.1111/j.1365-3091.1996.tb01509.x, 1996.

Chou, C., Formenti, P., Maille, M., Ausset, P., Helas, G., Harrison, M., and Osborne, S.: Size distribution, shape, and composition of mineral dust aerosols collected during the African Monsoon Multidisciplinary Analysis Special Observation Period 0: Dust and Biomass-Burning Experiment field campaign in Niger, January 2006, *J. Geophys. Res.*, 113, D00C10, doi:10.1029/2008jd009897, 2008.

Christidis, G. E.: Genesis and compositional heterogeneity of smectites. Part III: Alteration of basic pyroclastic rocks – a case study from the Troodos Ophiolite Complex, Cyprus, *Am. Mineral.*, 91, 685–701, 2006.

Christidis, G. E. and Dunham, A. C.: Compositional variations in smectites: Part I. Alteration of intermediate volcanic rocks. a case study from Milos Island, Greece, *Clay Miner.*, 28, 255–273, 1993.

Mapping the physico-chemical properties of mineral dust

P. Formenti et al.

Title Page

Abstract

Introduction

Conclusions

References

Tables

Figures

◀

▶

◀

▶

Back

Close

Full Screen / Esc

Printer-friendly Version

Interactive Discussion

- Claquin, T., Schulz, M., and Balkanski, Y. J.: Modeling the mineralogy of atmospheric dust sources, *J. Geophys. Res.*, 104, 22243–22256, 1999.
- Crowley, J. N., Ammann, M., Cox, R. A., Hynes, R. G., Jenkin, M. E., Mellouki, A., Rossi, M. J., Troe, J., and Wallington, T. J.: Evaluated kinetic and photochemical data for atmospheric chemistry: Volume V – heterogeneous reactions on solid substrates, *Atmos. Chem. Phys.*, 10, 9059–9223, doi:10.5194/acp-10-9059-2010, 2010.
- Cullen, M. J. P.: The unified forecast/climate model, *Meteorol. Mag.*, 122, 81–93, 1993.
- Dai, A.: Drought under global warming: a review, *Wiley Interdisciplinary Reviews: Climate Change*, 2, 45–65, doi:10.1002/wcc.81, 2011.
- De Souza-Machado, S., Strow, L. L., Motteler, H., and Hannon, S.: Infrared dust spectral signatures from AIRS, *Geophys. Res. Lett.*, 33, L03801, doi:10.1029/2005gl024364, 2006.
- Delany, A. C., Delany, A. C., Parkin, D. W., Griffin, J. J., Goldberg, E. D., and Reinmann, B. E. F.: Airborne dust collected at Barbados, *Geochim. Cosmochim. Ac.*, 31, 885–909, 1967.
- ECA (Economic Commission for Africa): Assessing sustainable development in Africa, *Africa's Sustainable Development Bulletin*, Economic Commission for Africa, Addis Ababa, 59 pp., 2005.
- Egan, W. G. and Hilgeman, T. W.: *Optical Properties of Inhomogeneous Materials: Applications to Geology, Astronomy, Chemistry, and Engineering*, Academic Press, Waltham, Massachusetts, 235 pp., 1979.
- Flamant, C., Lavaysse, C., Todd, M. C., Chaboureaud, J. P., and Pelon, J.: Multi-platform observations of a springtime case of Bodélé and Sudan dust emission, transport and scavenging over West Africa, *Q. J. Roy. Meteor. Soc.*, 135, 413–430, doi:10.1002/qj.376, 2009.
- Formenti, P., Elbert, W., Maenhaut, W., Haywood, J., and Andreae, M. O.: Chemical composition of mineral dust aerosol during the Saharan Dust Experiment (SHADE) airborne campaign in the Cape Verde region, September 2000, *J. Geophys. Res.*, 108, 8576, doi:10.1029/2002jd002648, 2003.
- Formenti, P., Rajot, J. L., Desboeufs, K., Caquineau, S., Chevaillier, S., Nava, S., Gaudichet, A., Journet, E., Triquet, S., Alfaro, S., Chiari, M., Haywood, J., Coe, H., and Highwood, E.: Regional variability of the composition of mineral dust from western Africa: results from the AMMA SOP0/DABEX and DODO field campaigns, *J. Geophys. Res.*, 113, D00C13, doi:10.1029/2008jd009903, 2008.
- Formenti, P., Nava, S., Prati, P., Chevaillier, S., Klaver, A., Lafon, S., Mazzei, F., Calzolari, G., and Chiari, M.: Self-attenuation artifacts and correction factors of light element measurements

Mapping the physico-chemical properties of mineral dust

P. Formenti et al.

Title Page

Abstract

Introduction

Conclusions

References

Tables

Figures

⏪

⏩

◀

▶

Back

Close

Full Screen / Esc

Printer-friendly Version

Interactive Discussion

by X-ray analysis: implication for mineral dust composition studies, *J. Geophys. Res.*, 115, D01203, doi:10.1029/2009jd012701, 2010.

Formenti, P., Schütz, L., Balkanski, Y., Desboeufs, K., Ebert, M., Kandler, K., Petzold, A., Scheuven, D., Weinbruch, S., and Zhang, D.: Recent progress in understanding physical and chemical properties of African and Asian mineral dust, *Atmos. Chem. Phys.*, 11, 8231–8256, doi:10.5194/acp-11-8231-2011, 2011a.

Formenti, P., Rajot, J. L., Desboeufs, K., Saïd, F., Grand, N., Chevaillier, S., and Schmechtig, C.: Airborne observations of mineral dust over western Africa in the summer Monsoon season: spatial and vertical variability of physico-chemical and optical properties, *Atmos. Chem. Phys.*, 11, 6387–6410, doi:10.5194/acp-11-6387-2011, 2011b.

Forster, P., Ramaswamy, V., Artaxo, P., Berntsen, T., Betts, R., Fahey, D. W., Haywood, J., Lean, J., Lowe, D. C., Myhre, G., Nganga, J., Prinn, R., Raga, G., Schulz, M., Van Dorland, R., Solomon, S., Qin, D., Manning, M., Chen, Z., Marquis, M., Averyt, K. B., Tignor, M., and Miller, H. L.: Changes in atmospheric constituents and in radiative forcing, in: *Climate Change 2007: The Physical Science Basis. Contribution of Working Group I to the Fourth Assessment Report of the Intergovernmental Panel on Climate Change*, edited by: Solomon, S. et al., Cambridge Univ. Press, Cambridge, UK, 129–234, 2007.

Gillette, D. and Walker, T. R.: Characteristics of airborne particles produced by wind erosion of sandy soil, high plains of West Texas, *Soil Sci.*, 123, 97–110, 1977.

Glaccum, R. A. and Prospero, J. M.: Saharan aerosols over the tropical north Atlantic – mineralogy, *Mar. Geol.*, 37, 295–321, 1980.

Glotch, T. D. and Rossman, G. R.: Mid-infrared reflectance spectra and optical constants of six iron oxide/oxyhydroxide phases, *Icarus*, 204, 663–671, 2009.

Glotch, T. D., Rossman, G. R., and Aharonson, O.: Mid-infrared (5–100 μm) reflectance spectra and optical constants of ten phyllosilicate minerals, *Icarus*, 192, 604–622, doi:10.1016/j.icarus.2007.07.002, 2007.

Goudie, A. S. and Middleton, N. J.: Saharan dust storms: nature and consequences, *Earth-Sci. Rev.*, 56, 179–204, 2001.

Gustafsson, R. J., Orlov, A., Griffiths, P. T., Cox, R. A., and Lambert, R. M.: Reduction of NO_2 to nitrous acid on illuminated titanium dioxide aerosol surfaces: implications for photocatalysis and atmospheric chemistry, *Chem. Commun.*, 5, 3936–3938, 2006.

Hansell Jr., R. A., Reid, J. S., Tsay, S. C., Roush, T. L., and Kalashnikova, O. V.: A sensitivity study on the effects of particle chemistry, asphericity and size on the mass extinction effi-

Mapping the physico-chemical properties of mineral dust

P. Formenti et al.

Title Page

Abstract

Introduction

Conclusions

References

Tables

Figures

◀

▶

◀

▶

Back

Close

Full Screen / Esc

Printer-friendly Version

Interactive Discussion

ciency of mineral dust in the earth's atmosphere: from the near to thermal IR, *Atmos. Chem. Phys.*, 11, 1527–1547, doi:10.5194/acp-11-1527-2011, 2011.

Haywood, J. M., Allan, R. P., Culverwell, I., Slingo, T., Milton, S., Edwards, J., and Clerbaux, N.: Can desert dust explain the outgoing longwave radiation anomaly over the Sahara during July 2003?, *J. Geophys. Res.*, 110, D05105, doi:10.1029/2004JD005232, 2005.

Haywood, J. M., Pelon, J., Formenti, P., Bharmal, N., Brooks, M., Capes, G., Chazette, P., Chou, C., Christopher, S., Coe, H., Cuesta, J., Derimian, Y., Desboeufs, K., Greed, G., Harrison, M., Heese, B., Highwood, E. J., Johnson, B., Mallet, M., Marticorena, B., Marsham, J., Milton, S., Myhre, G., Osborne, S. R., Parker, D. J., Rajot, J. L., Schulz, M., Slingo, A., Tanré, D., and Tulet, P.: Overview of the dust and biomass-burning experiment and African monsoon multidisciplinary analysis special observing period-0, *J. Geophys. Res.*, 113, D00C17, doi:10.1029/2008jd010077, 2008.

Haywood, J. M., Johnson, B. T., Osborne, S. R., Baran, A. J., Brooks, M., Milton, S. F., Mulcahy, J., Walters, D., Allan, R. P., Klaver, A., Formenti, P., Brindley, H. E., Christopher, S., and Gupta, P.: Motivation, rationale and key results from the GERBILS Saharan dust measurement campaign, *Q. J. Roy. Meteor. Soc.*, 137, 1106–1116, doi:10.1002/qj.797, 2011.

Heintzenberg, J.: The SAMUM-1 experiment over southern Morocco: overview and introduction, *Tellus B*, 61, 2–11, doi:10.1111/j.1600-0889.2008.00403.x, 2008.

Hess, M., Koepke, P., and Schult, I.: Optical properties of aerosols and clouds: the software package OPAC, *B. Am. Meteorol. Soc.*, 79, 831–844, 1998.

Highwood, E. J., Haywood, J. M., Silverstone, M. D., Newman, S. M., and Taylor, J. P.: Radiative properties and direct effect of Saharan dust measured by the C-130 aircraft during Saharan Dust Experiment (SHADE): 2. Terrestrial spectrum, *J. Geophys. Res.*, 108, 8578, doi:10.1029/2002JD002552, 2003.

Hinds, W. C.: *Aerosol Technology: Properties, Behavior, and Measurement of Airborne Particles*, John Wiley & Sons, Chichester, 504 pp., 1999.

Hoose, C., Lohmann, U., Erdin, R., and Tegen, I.: The global influence of dust mineralogical composition on heterogeneous ice nucleation in mixed-phase clouds, *Environ. Res. Lett.*, 3, 025003, doi:10.1088/1748-9326/3/2/025003, 2008.

Hower, J. and Mowatt, T. C.: The Mineralogy of illites and mixed-layer illite/Montmorillonites, *Am. Mineral.*, 51, 825–854, 1966.

Mapping the physico-chemical properties of mineral dust

P. Formenti et al.

Title Page

Abstract

Introduction

Conclusions

References

Tables

Figures

◀

▶

◀

▶

Back

Close

Full Screen / Esc

Printer-friendly Version

Interactive Discussion

Hudson, P. K., Gibson, E. R., Young, M. A., Kleiber, P. D., and Grassian, V. H.: Coupled infrared extinction and size distribution measurements for several clay components of mineral dust aerosol, *J. Geophys. Res.*, 113, D01201, doi:10.1029/2007JD008791, 2008a.

Hudson, P. K., Young, M. A., Kleiber, P. D., and Grassian, V. H.: coupled infrared extinction spectra and size distribution measurements for several non-clay components of mineral dust aerosol (quartz, calcite, and dolomite), *Atmos. Environ.*, 42, 5991–5999, 2008b.

Huneeus, N., Schulz, M., Balkanski, Y., Griesfeller, J., Prospero, J., Kinne, S., Bauer, S., Boucher, O., Chin, M., Dentener, F., Diehl, T., Easter, R., Fillmore, D., Ghan, S., Ginoux, P., Grini, A., Horowitz, L., Koch, D., Krol, M. C., Landing, W., Liu, X., Mahowald, N., Miller, R., Morcrette, J.-J., Myhre, G., Penner, J., Perlwitz, J., Stier, P., Takemura, T., and Zender, C. S.: Global dust model intercomparison in AeroCom phase I, *Atmos. Chem. Phys.*, 11, 7781–7816, doi:10.5194/acp-11-7781-2011, 2011.

Janicot, S., Thorncroft, C. D., Ali, A., Asencio, N., Berry, G., Bock, O., Bourles, B., Caniaux, G., Chauvin, F., Deme, A., Kergoat, L., Lafore, J.-P., Lavaysse, C., Lebel, T., Marticorena, B., Mounier, F., Nedelec, P., Redelsperger, J.-L., Ravegnani, F., Reeves, C. E., Roca, R., de Rosnay, P., Schlager, H., Sultan, B., Tomasini, M., Ulanovsky, A., and ACMAD forecasters team: Large-scale overview of the summer monsoon over West Africa during the AMMA field experiment in 2006, *Ann. Geophys.*, 26, 2569–2595, doi:10.5194/angeo-26-2569-2008, 2008.

Jickells, T. D., An, Z. S., Andersen, K. K., Baker, A. R., Bergametti, G., Brooks, N., Cao, J. J., Boyd, P. W., Duce, R. A., Hunter, K. A., Kawahata, H., Kubilay, N., laRoche, J., Liss, P. S., Mahowald, N., Prospero, J. M., Ridgwell, A. J., Tegen, I., and Torres, R.: Global iron connections between desert dust, ocean biogeochemistry, and climate, *Science*, 308, 67–71, doi:10.1126/science.1105959, 2005.

Johnson, B. T., Osborne, S. R., Haywood, J. M., and Harrison, M. A. J.: Aircraft measurements of biomass burning aerosol over West Africa during DABEX, *J. Geophys. Res.*, 113, D00C06, doi:10.1029/2007jd009451, 2008.

Journet, E., Desboeufs, K. V., Caquineau, S., and Colin, J.-L.: Mineralogy as a critical factor of dust iron solubility, *Geophys. Res. Lett.*, 35, L07805, doi:10.1029/2007gl031589, 2008.

Journet, E., Balkanski, Y., and Harrison, S. P.: A new data set of soil mineralogy for dust-cycle modeling, *Atmos. Chem. Phys. Discuss.*, 13, 23943–23993, doi:10.5194/acpd-13-23943-2013, 2013.

Kandler, K., Schütz, L., Deutscher, C., Ebert, M., Hofmann, H., Jäckel, S., Jaenicke, R., Knipertz, P., Lieke, K., Massling, A., Petzold, A., Schladitz, A., Weinzierl, B., Wiedensohler, A.,

Mapping the physico-chemical properties of mineral dust

P. Formenti et al.

Title Page

Abstract

Introduction

Conclusions

References

Tables

Figures

⏪

⏩

◀

▶

Back

Close

Full Screen / Esc

Printer-friendly Version

Interactive Discussion

Zorn, S., and Weinbruch, S.: Size distribution, mass concentration, chemical and mineralogical composition and derived optical parameters of the boundary layer aerosol at Tinfou, Morocco, during SAMUM 2006, *Tellus B*, 61, 32–50, doi:10.1111/j.1600-0889.2008.00385.x, 2009.

- 5 Karickhoff, S. W. and Bailey, G. W.: Optical absorption spectra of clay minerals, *Clay. Clay Miner.*, 21, 59–70, 1973.
- Kiefert, L., McTainsh, G. H., and Nickling, W. G.: Sedimentological characteristics of Saharan and Australian dust, in: *The Impact of Desert Dust Across the Mediterranean*, edited by: Guerzoni, S. and Chester, R., Kluwer Acad., Norwell, Mass., 183–190, 1996.
- 10 Klaver, A., Formenti, P., Caquineau, S., Chevaillier, S., Ausset, P., Calzolari, G., Osborne, S., Johnson, B., Harrison, M., and Dubovik, O.: Physico-chemical and optical properties of Sahelian and Saharan mineral dust: in situ measurements during the GERBILS campaign, *Q. J. Roy. Meteor. Soc.*, 137, 1193–1210, doi:10.1002/qj.889, 2011.
- Klaver, A.: Estimation des propriétés optiques des poussières désertiques d'origines saharienne et sahélienne, à proximité de leurs zones sources d'émission, à partir de leurs propriétés physico-chimiques, thèse de Doctorat, Université Paris VII, Paris, 2012.
- Klüser, L. and Schepanski, K.: Remote sensing of mineral dust over land with MSG infrared channels: a new Bitemporal Mineral Dust Index, *Remote Sens. Environ.*, 113, 1853–1867, 2009.
- 20 Klüser, L., Martynenko, D., and Holzer-Popp, T.: Thermal infrared remote sensing of mineral dust over land and ocean: a spectral SVD based retrieval approach for IASI, *Atmos. Meas. Tech.*, 4, 757–773, doi:10.5194/amt-4-757-2011, 2011.
- Klüser, L., Kleiber, P., Holzer-Popp, T., and Grassian, V. H.: Desert dust observation from space – application of measured mineral component infrared extinction spectra, *Atmos. Environ.*, 25, 54, 419–427, 2012.
- Köster, H. M., Ehrlicher, U., Gilg, H. A., Jordan, R., Murad, E., and Onnich, K.: Mineralogical and chemical characteristics of five nontronites and Fe-rich smectites, *Clay Miner.*, 34, 579–599, 1999.
- 30 Koren, I., Kaufman, Y. J., Washington, R., Todd, M. C., Rudich, Y., Vanderlei Martins, J., and Rosenfeld, D.: The Bodélé depression: a single spot in the Sahara that provides most of the mineral dust to the Amazon forest, *Environ. Res. Lett.*, 1, 014005, doi:10.1088/1748-9326/1/1/014005, 2006.

**Mapping the
physico-chemical
properties of mineral
dust**

P. Formenti et al.

Title Page

Abstract

Introduction

Conclusions

References

Tables

Figures

◀

▶

◀

▶

Back

Close

Full Screen / Esc

Printer-friendly Version

Interactive Discussion



- Lafon, S., Rajot, J., Alfaro, S., and Gaudichet, A.: Quantification of iron oxides in desert aerosol, *Atmos. Environ.*, 38, 1211–1218, 2004.
- Lafon, S., Sokolik, I. N., Rajot, J. L., Caquineau, S., and Gaudichet, A.: Characterization of iron oxides in mineral dust aerosols: implications for light absorption, *J. Geophys. Res.*, 111, D21207, doi:10.1029/2005jd007016, 2006.
- Laskina, O., Young, M. A., Kleiber, P. D., and Grassian, V. H.: Infrared extinction spectra of mineral dust aerosol: single components and complex mixtures, *J. Geophys. Res.*, 117, D18210, doi:10.1029/2012JD017756, 2012
- Laurent, B., Marticorena, B., Bergametti, G., Léon, J. F., and Mahowald, N. M.: Modeling mineral dust emissions from the Sahara desert using new surface properties and soil database, *J. Geophys. Res.*, 113, D14218, doi:10.1029/2007jd009484, 2008.
- Lazaro, F. J., Gutiérrez, L., Barrón, V., and Gelado, M. D.: The speciation of iron in desert dust collected in Gran Canaria (Canary Islands): combined chemical, magnetic and optical analysis, *Atmos. Environ.*, 42, 8987–8996, 2008.
- Lebel, T., Parker, D. J., Flamant, C., Bourlès, B., Marticorena, B., Mougín, E., Peugeot, C., Diedhiou, A., Haywood, J. M., Ngamini, J. B., Polcher, J., Redelsperger, J. L., and Thornicroft, C. D.: The AMMA field campaigns: multiscale and multidisciplinary observations in the West African region, *Q. J. Roy. Meteor. Soc.*, 136, 8–33, doi:10.1002/qj.486, 2010.
- Legrand, M., N'doumé, C., and Jankowiak, I.: Satellite-derived climatology of the Saharan aerosol., in: *Passive Infrared Remote Sensing of Clouds and the Atmosphere II*, edited by: Lynch, D. K., *Proc. SPIE* 2309, 127–135, 1994.
- Lepple, F. K. and Brine, C. J.: Organic constituents in eolian dust and surface sediments from northwest Africa, *J. Geophys. Res.*, 81, 1141–1147, 1976.
- Long, L. L., Querry, M. R., Bell, R. J., and Alexander, R. W.: Optical properties of calcite and gypsum in crystalline and powdered form in the infrared and far-infrared, *Infrared Phys.*, 34, 191–201, 1993.
- Longtin, D. R., Shettle, E. P., Hummel, J. R., and Pryce, J. D.: *A Wind Dependent Desert Aerosol Model: Radiative Properties*, AFGL-TR-88-0112, Air Force Geophysics Laboratory, Hanscom AFB, MA, 1988.
- Mahowald, N.: Aerosol indirect effects on biogeochemistry and climate, *Science*, 334, 794, doi:10.1126/science.1207374, 2011.

**Mapping the
physico-chemical
properties of mineral
dust**

P. Formenti et al.

Title Page

Abstract

Introduction

Conclusions

References

Tables

Figures

◀

▶

◀

▶

Back

Close

Full Screen / Esc

Printer-friendly Version

Interactive Discussion



- Majestic, B. J., Schauer, J. J., and Shafer, M. M.: Application of synchrotron radiation for measurement of iron red-ox speciation in atmospherically processed aerosols, *Atmos. Chem. Phys.*, 7, 2475–2487, doi:10.5194/acp-7-2475-2007, 2007.
- Marra, A. C., Blanco, A., Fonti, S., Jurewicz, A., and Orfino, V.: Fine hematite particles of Martian interest: absorption spectra and optical constants, *J. Phys. Conf. Ser.*, 6, 132–138, 2005.
- Marticorena, B., and Bergametti, G.: Modeling the atmospheric dust cycle: 1. Design of a soil-derived dust emission scheme, *J. Geophys. Res.*, 100, 16415–16430, doi:10.1029/95jd00690, 1995.
- Marticorena, B., Chatenet, B., Rajot, J. L., Traoré, S., Coulibaly, M., Diallo, A., Koné, I., Maman, A., NDiaye, T., and Zakou, A.: Temporal variability of mineral dust concentrations over West Africa: analyses of a pluriannual monitoring from the AMMA Sahelian Dust Transect, *Atmos. Chem. Phys.*, 10, 8899–8915, doi:10.5194/acp-10-8899-2010, 2010.
- Mason, B.: *Principles of Geochemistry*, 3rd edn., John Wiley, New York, 1966.
- McConnell, C. L., Highwood, E. J., Coe, H., Formenti, P., Anderson, B., Osborne, S., Nava, S., Desboeufs, K., Chen, G., and Harrison, M. A. J.: Seasonal variations of the physical and optical characteristics of Saharan dust: results from the Dust Outflow and Deposition to the Ocean (DODO) experiment, *J. Geophys. Res.*, 113, D14S05, doi:10.1029/2007jd009606, 2008.
- McConnell, C. L., Formenti, P., Highwood, E. J., and Harrison, M. A. J.: Using aircraft measurements to determine the refractive index of Saharan dust during the DODO Experiments, *Atmos. Chem. Phys.*, 10, 3081–3098, doi:10.5194/acp-10-3081-2010, 2010.
- Mehra, O. P. and Jackson, M. L.: Iron oxide removal from soils and clays by a dithionite-citrate buffered with sodium bicarbonate, *Clay Miner.*, 7, 317–327, 1960.
- Mestdagh, M. M., Vielvoye, L., and Herbillon, A. J.: Iron in Kaolinite: the relationship between kaolinite crystallinity and iron content, *Clay Miner.*, 15, 1–13, 1980.
- Mogili, P. K., Yang, K. H., Young, M. A., Kleiber, P. D., and Grassian, V. H.: Environmental aerosol chamber studies of extinction spectra of mineral dust aerosol components: broadband IR-UV extinction spectra, *J. Geophys. Res.-Atmos.*, 112, D21204, doi:10.1029/2007jd008890, 2007.
- Mogili, P. K., Yang, K. H., Young, M. A., Kleiber, P. D., and Grassian, V. H.: Extinction spectra of mineral dust aerosol components in an environmental aerosol chamber: IR resonance studies, *Atmos. Environ.*, 42, 1752–1761, doi:10.1016/j.atmosenv.2007.11.026, 2008.

**Mapping the
physico-chemical
properties of mineral
dust**

P. Formenti et al.

Title Page

Abstract

Introduction

Conclusions

References

Tables

Figures

◀

▶

◀

▶

Back

Close

Full Screen / Esc

Printer-friendly Version

Interactive Discussion

- Mooney, T. and Knacke, R. F.: Optical constants of chlorite and serpentine between 2.5 and 50 μm , *Icarus*, 64, 493–502, 1985.
- Müller, T., Schladitz, A., Massling, A., Kaaden, N., Kandler, K., and Wiedensohler, A.: Spectral absorption coefficients and imaginary parts of refractive indices of Saharan dust during SAMUM-1, *Tellus B*, 61, 79–95, doi:10.1111/j.1600-0889.2008.00399.x, 2009.
- Murad, E. and Wagner, U.: The Mossbauer spectrum of illite, *Clay Miner.*, 29, 1–10, 1994.
- Ndour, M., D'Anna, B., George, C., Ka, O., Balkanski, Y., Kleffmann, J., Stemmler, K., and Ammann, M.: Photoenhanced uptake of NO_2 on mineral dust: laboratory experiments and model simulations, *Geophys. Res. Lett.*, 35, L05812, doi:10.1029/2007GL032006, 2008.
- Nickovic, S., Vukovic, A., Vujadinovic, M., Djurdjevic, V., and Pejanovic, G.: Technical Note: High-resolution mineralogical database of dust-productive soils for atmospheric dust modeling, *Atmos. Chem. Phys.*, 12, 845–855, doi:10.5194/acp-12-845-2012, 2012.
- N'Tchayi, G. M., Bertrand, J., Legrand, M., and Baudet, J.: Temporal and spatial variations of the atmospheric dust loading throughout West Africa over the last thirty years, *Ann. Geophys.*, 12, 265–273, doi:10.1007/s00585-994-0265-3, 1994.
- N'Tchayi Mbourou, G., Bertrand, J., and Nicholson, S. E.: The diurnal and seasonal cycles of wind-borne dust over Africa north of the equator, *J. Appl. Meteorol.*, 36, 868–882, 1997.
- O'Day, P. A., Rivera, N., Root, R., and Carroll, S. A.: X-ray absorption spectroscopic study of Fe reference compounds for the analysis of natural sediments, *Am. Mineral.*, 89, 572–585, 2004.
- Ohta, A., Tsuno, H., Kagi, H., Kanai, Y., Nomura, M., Zhang, R., Terashima, N., and Imai, N.: Chemical compositions and XANES speciations of Fe, Mn and Zn from aerosols collected in China and Japan during dust events, *Geochem. J.*, 40, 363–376, 2006.
- Paquet, H., Coudé-Gaussen, G., and Rognon, P.: Etude minéralogique de poussières sahariennes le long d'un itinéraire entre 19° et 35° de latitude nord, *Rev. Geol. Dyn. Geogr.*, 25, 257–265, 1984.
- Paris, R., Desboeufs, K. V., and Journet, E.: Variability of dust iron solubility in atmospheric waters: investigation of the role of oxalate organic complexation, *Atmos. Environ.*, 45, 6510–6517, doi:10.1016/j.atmosenv.2011.08.068, 2011.
- Patterson, E., Gillette, D., and Stockton, B.: Complex index of refraction between 300 and 700 nm for Saharan aerosols, *J. Geophys. Res.*, 82, 3153–3160, 1977.
- Pentakov, L., Su, K., Pentak, M., and Stucki, J. W.: A review of microbial redox interactions with structural Fe in clay minerals, *Clay Miner.*, 48, 543–560, 2013.

Mapping the physico-chemical properties of mineral dust

P. Formenti et al.

Title Page

Abstract

Introduction

Conclusions

References

Tables

Figures

⏪

⏩

◀

▶

Back

Close

Full Screen / Esc

Printer-friendly Version

Interactive Discussion

- Peterson, J. T. and Weinman, J. A.: Optical properties of quartz dust particles at infrared wavelengths, *J. Geophys. Res.*, 74, 6947–6952, 1969.
- Prietzl, J., Thieme, J., Eusterhues, K., and Eichert, D.: Iron speciation in soils and soil aggregates by synchrotron-based x. ray microspectroscopy (xanes, mu-xanes), *Eur. J. Soil Sci.*, 58, 1027–1041, 2007.
- Prospero, J. M., Ginoux, P., Torres, O., Nicholson, S. E., and Gill, T. E.: Environmental characterization of global sources of atmospheric soil dust identified with the Nimbus 7 Total Ozone Mapping Spectrometer (TOMS) absorbing aerosol product, *Rev. Geophys.*, 40, 2-1–2-31, 2002.
- Pye, K.: *Aeolian Dust and Dust Deposits*, Academic Press, London, 334 pp., 1987.
- Querry, M. R.: *Optical Constants of Minerals and Other Materials From the Millimeter to the UV*. US Army Rep. CRDEC-CR- 88009, Aberdeen, MD, 1987.
- Querry, M. R., Osborne, G., Lies, K., Jordon, R., and Coveney, R. M.: Complex refractive index of limestone in the visible and infrared, *Appl. Optics*, 17, 353–356, 1978.
- Rahn, K. A.: Silicon and aluminum in atmospheric aerosols: crust-air fractionation?, *Atmos. Environ.*, 10, 597–601, 1976.
- Rajot, J.-L.: Wind blown sediment mass budget of Sahelian village land units in Niger, *B. Soc. Geol. Fr.*, 172, 523–531, 2001.
- Rajot, J. L., Formenti, P., Alfaro, S., Desboeufs, K., Chevaillier, S., Chatenet, B., Gaudichet, A., Journet, E., Marticorena, B., Triquet, S., Maman, A., Mouget, N., and Zakou, A.: AMMA dust experiment: an overview of measurements performed during the dry season special observation period (SOP0) at the Banizoumbou (Niger) supersite, *J. Geophys. Res.*, 113, D00C14, doi:10.1029/2008jd009906, 2008.
- Redelsperger, J.-L., Thorncroft, C. D., Diedhiou, A., Lebel, T., Parker, D. J., and Polcher, J.: African monsoon multidisciplinary analysis: an international research project and field campaign, *B. Am. Meteorol. Soc.*, 87, 1739–1746, doi:10.1175/BAMS-87-12-1739, 2006.
- Reeves, C. E., Formenti, P., Afif, C., Ancellet, G., Attié, J.-L., Bechara, J., Borbon, A., Cairo, F., Coe, H., Crumeyrolle, S., Fierli, F., Flamant, C., Gomes, L., Hamburger, T., Lambert, C., Law, K. S., Mari, C., Jones, R. L., Matsuki, A., Mead, M. I., Methven, J., Mills, G. P., Minikin, A., Murphy, J. G., Nielsen, J. K., Oram, D. E., Parker, D. J., Richter, A., Schlager, H., Schwarzenboeck, A., and Thouret, V.: Chemical and aerosol characterisation of the troposphere over West Africa during the monsoon period as part of AMMA, *Atmos. Chem. Phys.*, 10, 7575–7601, doi:10.5194/acp-10-7575-2010, 2010.

**Mapping the
physico-chemical
properties of mineral
dust**P. Formenti et al.

[Title Page](#)[Abstract](#)[Introduction](#)[Conclusions](#)[References](#)[Tables](#)[Figures](#)[◀](#)[▶](#)[◀](#)[▶](#)[Back](#)[Close](#)[Full Screen / Esc](#)[Printer-friendly Version](#)[Interactive Discussion](#)

- Reid, E. A., Reid, J. S., Meier, M. M., Dunlap, M. R., Cliff, S. S., Broumas, A., Perry, K., and Maring, H.: Characterization of African dust transported to Puerto Rico by individual particle and size segregated bulk analysis, *J. Geophys. Res.*, 108, 8591, doi:10.1029/2002jd002935, 2003.
- 5 Saïd, F., Canut, G., Durand, P., Lohou, F., and Lathon, M.: Seasonal evolution of boundary-layer turbulence measured by aircraft during the AMMA 2006 Special Observation Period, *Q. J. Roy. Meteor. Soc.*, 136, 47–65, doi:10.1002/qj.475, 2010.
- Schepanski, K., Tegen, I., Laurent, B., Heinold, B., and Macke, A.: A new Saharan dust source activation frequency map derived from MSG-SEVIRI IR channels, *Geophys. Res. Lett.*, 34, L18803, doi:10.1029/2007GL030168, 2007.
- 10 Schepanski, K., Tegen, I., Todd, M. C., Heinold, B., Bönisch, G., Laurent, B., and Macke, A.: Meteorological processes forcing Saharan dust emission inferred from MSG-SEVIRI observations of subdaily dust source activation and numerical models, *J. Geophys. Res.*, 114, D10201, doi:10.1029/2008jd010325, 2009.
- 15 Schepanski, K., Tegen, I., and Macke, A.: Comparison of satellite based observations of Saharan dust source areas, *Remote Sens. Environ.*, 123, 90–97, 2012.
- Scheuven, D., Schütz, L., Kandler, K., Ebert, M., and Weinbruch, S.: Bulk composition of northern African dust and its source sediments – a compilation, *Earth-Sci. Rev.*, 116, 170–194, doi:10.1016/j.earscirev.2012.08.005, 2013.
- 20 Schroth, A. W., Crusius, J., Sholkovitz, E. R., and Bostick, B. C.: Iron solubility driven by speciation in dust sources to the ocean, *Nat. Geosci.*, 2, 337–340, 2009.
- Shao, Y., Wyrwoll, K.-H., Chappell, A., Huang, J., Lin, Z., McTainsh, G. H., Mikami, M., Tanaka, T. Y., Wang, X., and Yoon, S.: Dust cycle: an emerging core theme in Earth system science, *Aeolian Research*, 2, 181–204, doi:10.1016/j.aeolia.2011.02.001, 2011.
- 25 Shettle, E. P. and Fenn, R. W.: Models for the aerosols of the lower atmosphere and the effects of humidity variations on their optical properties. U.S. Air Force Geophysics Laboratory, Hanscomb Air Force Base, Mass., Air Force Geophysics Laboratory, 1979.
- Smith, A. J. A. and Grainger, R. G.: Does variation in mineral composition alter the short-wave light scattering properties of desert dust aerosol?, *J. Quant. Spectrosc. Ra.*, 133, 235–243, doi:10.1016/j.jqsrt.2013.08.005, 2013.
- 30 Sokolik, I. and Toon, O.: Incorporation of mineralogical composition into models of the radiative properties of mineral aerosol from UV to IR wavelengths, *J. Geophys. Res.*, 104, 9423–9444, 1999.

**Mapping the
physico-chemical
properties of mineral
dust**

P. Formenti et al.

Title Page

Abstract

Introduction

Conclusions

References

Tables

Figures

◀

▶

◀

▶

Back

Close

Full Screen / Esc

Printer-friendly Version

Interactive Discussion

Sokolik, I. N., Toon, O. B., and Bergstrom, R. W.: Modeling the radiative characteristics of airborne mineral aerosols at infrared wavelengths. *Journal of Geophys. Res. Lett.*, 103, 8813–8826, 1998.

5 Sokolik, I. N., Winker, D. M., Bergametti, G., Gillette, D. A., Carmichael, G., Kaufman, Y. J., Gomes, L., Schuetz, L., and Penner, J. E.: Introduction to special section: outstanding problems in quantifying the radiative impacts of mineral dust, *J. Geophys. Res.*, 106, 18015–18027, doi:10.1029/2000jd900498, 2001.

Sow, M., Alfaro, S. C., Rajot, J. L., and Marticorena, B.: Size resolved dust emission fluxes measured in Niger during 3 dust storms of the AMMA experiment, *Atmos. Chem. Phys.*, 9, 3881–3891, doi:10.5194/acp-9-3881-2009, 2009.

10 Spitzer, W. G. and Kleinman, D. A.: Infrared lattice bands of quartz, *Phys. Rev.*, 121, 1324–1335, 1961.

Tegen, I. and Fung, I.: Modeling of mineral dust in the atmosphere: sources, transport, and optical thickness, *J. Geophys. Res.*, 99, 22897–22914, 1994.

15 Toon, O. B., Pollock, J. B., and Khare, B. N.: The optical constants of several atmospheric aerosols species: ammonium sulfate, aluminum oxide and sodium chloride, *J. Geophys. Res. Lett.*, 81, 5733–5748, 1976.

Tulet, P., Mallet, M., Pont, V., Pelon, J., and Boone, A.: The 7–13 March 2006 dust storm over West Africa: generation, transport, and vertical stratification, *J. Geophys. Res.*, 113, D00C08, doi:10.1029/2008jd009871, 2008.

20 Washington, R., Todd, M., Middleton, N. J., and Goudie, A. S.: Dust-storm source areas determined by the total ozone monitoring spectrometer and surface observations, *Ann. Assoc. Am. Geogr.*, 93, 297–313, 2003.

Washington, R., Todd, M. C., Engelstaedter, S., Mbainayel, S., and Mitchell, F.: Dust and the low-level circulation over the Bodélé Depression, Chad: observations from BoDEX 2005, *J. Geophys. Res.*, 111, D03201, doi:10.1029/2005jd006502, 2006.

25 Washington, R., Flamant, C., Parker, D. J., Marsham, J., McQuaid, J. B., Brindley, H., Todd, M., Highwood, E. J., Chaboureaud, J.-P., Kocha, C., Bechir, M., Saci, A., and Ryder, C. L.: Fennec – The Saharan Climate System, *CLIVAR Exchanges*, 60, 31–33, 2012.

30 Wilke, M., Farges, F., Petit, P.-E., Brown, G. E. J., and Mertin, F.: Oxidation state and coordination of Fe in minerals: an Fe K-XANES spectroscopic study, *Am. Mineral.*, 86, 714–730, 2001.

Yoshioka, M., Mahowald, N., Dufresne, J.-L., and Luo, C.: Simulation of absorbing aerosol indices for African dust, *J. Geophys. Res.*, 110, D18S17, doi:10.1029/2004jd005276, 2005.

ACPD

14, 10241–10310, 2014

**Mapping the
physico-chemical
properties of mineral
dust**

P. Formenti et al.

Title Page

Abstract

Introduction

Conclusions

References

Tables

Figures



Back

Close

Full Screen / Esc

Printer-friendly Version

Interactive Discussion



Mapping the physico-chemical properties of mineral dust

P. Formenti et al.

Title Page

Abstract

Introduction

Conclusions

References

Tables

Figures

⏪

⏩

◀

▶

Back

Close

Full Screen / Esc

Printer-friendly Version

Interactive Discussion

Table 1. Calibration coefficients by mineral obtained for the calibration of the XRD analyser used in this study. The calibration coefficients represent the slope of the correlation line between the number of diffracted counts by unit mass. The references of the standard minerals used in this study are also reported.

Mineral	Origin	Slope (cpsmg ⁻¹)	<i>R</i> ²
Quartz (SiO ₂)	Fontainebleau, France	446 ± 14 (3 %)	0.88
Calcite (CaCO ₃)	Bédarieux, France	325 ± 11 (3 %)	0.94
Dolomite (CaMg(CO ₃) ₂)	Traversella, Italie	679 ± 70 (10 %)	0.55
Gypsum (CaSO ₄ · 2H ₂ O)	Unknown	446 ± 22 (5 %)	0.89
Orthose (KAlSi ₃ O ₈)	Madagascar	997 ± 70 (7 %)	0.69
Albite (NaAlSi ₃ O ₈)	Ontario, Canada	2456 ± 56 (2 %)	0.96

Mapping the physico-chemical properties of mineral dust

P. Formenti et al.

Title Page

Abstract

Introduction

Conclusions

References

Tables

Figures

◀

▶

◀

▶

Back

Close

Full Screen / Esc

Printer-friendly Version

Interactive Discussion



Table 2. Mean values of the relative proportions of iron in the form of hematite and goethite to total iron oxide as obtained by XAS/XANES analysis. Standard deviations are indicated in parenthesis.

Origin	Fe as oxide	Fe oxide as goethite	Fe oxide as hematite
Bodélé	43 % (11 %)	65 % (7 %)	35 % (7 %)
North Niger	57 % (2 %)	59 % (8 %)	41 % (8 %)
South Algeria	55 % (–)	62 % (–)	38 % (–)
Erosion, Sahel	66 % (5 %)	68 % (5 %)	32 % (5 %)

Mapping the physico-chemical properties of mineral dust

P. Formenti et al.

Table 3. Mineralogical composition (percentage by mass, in %) according to the source region. Standard deviations are indicated in parenthesis.

Source	Kaolinite	Illite	Quartz	Orthose	Albite	Calcite	Dolomite	Gypsum	Goethite	Hematite	Titanium oxide
Bodélé (wintertime)	84.1 (–)	8.5 (–)	2.9 (–)	0.2 (–)	< DL	0.9 (–)	< DL	0.2 (–)	1.6 (–)	1.1 (–)	0.7
Bodélé/Sudan (summertime)	76.1 (4.4)	7.0 (0.4)	11.2 (5.6)	0.5 (0.2)	0.1 (0.1)	1.3 (0.8)	0.3 (0.1)	0.2 (–)	2.0 (0.3)	1.3 (0.3)	0.7
North Niger/Libya	54.0 (–)	37.8 (–)	4.6 (–)	0.2 (–)	< DL	0.4 (–)	< DL	< DL	1.5 (–)	0.8 (–)	0.8
North Niger/Libya/south Algeria	60.5 (4.7)	24.0 (1.9)	3.6 (3.1)	0.2 (–)	< DL	6.3 (2.9)	< DL	< DL	3.1 (0.2)	1.6 (0.1)	0.8
South Algeria/Mali	71.1 (13.5)	16.4 (11.8)	7.1 (0.8)	0.4 (0.2)	0.2 (0.1)	1.5 (0.01)	0.7 (0.4)	0.3 (–)	1.1 (0.1)	0.8 (0.05)	0.8
South Algeria/North Niger (smectites)	75.2 (3)	7.0 (0.3)	10.8 (2.0)	0.6 (0.2)	0.1 (0.1)	0.9 (0.6)	0.4 (0.2)	0.5 (–)	2.4 (0.6)	1.7 (0.4)	0.8
South Algeria/North Niger (non smectites)	78.2 (2.2)	7.2 (0.2)	6.6 (0.7)	0.4 (0.1)	0.1 (0.02)	3.0 (3.6)	0.2 (0.05)	0.6 (0.3)	2.4 (1.5)	1.8 (1.1)	0.8
North Niger	78.3 (–)	7.4 (–)	9.7 (–)	0.5 (–)	0.1 (–)	< DL	0.3 (–)	0.9 (–)	1.4 (–)	0.7 (–)	0.8
Local erosion (all)	73.0 (13)	7.1 (1.3)	14.3 (13)	0.8 (1)	0.1 (0.2)	< DL	0.1 (–)	0.3 (0.3)	2.1 (0.5)	1.2 (0.4)	1.3
Local erosion (quartz-rich)	46.6 (–)	4.4 (–)	40.6 (–)	2.9 (–)	0.4 (–)	< DL	< DL	< DL	2.4 (–)	1.4 (–)	1.4
Local erosion (excluding quartz-rich)	78.3 (1.5)	7.5 (0.2)	9.1 (2.2)	0.4 (0.1)	< DL	< DL	0.1 (–)	0.3 (0.3)	2.0 (0.6)	1.1 (0.4)	1.4
Mali/Mauritania	29.7 (–)	46.3 (–)	17.3 (–)	1.3 (–)	0.4 (–)	1.0 (–)	0.8 (–)	< DL	1.3 (–)	0.7 (–)	1.3
Mali/Mauritania/western Sahara	30.7 (3.2)	54.2 (6.0)	8.4 (1.7)	0.3 (0.1)	0.2 (0.2)	1.2 (0.9)	0.2 (0.2)	0.4 (–)	2.0 (0.5)	1.3 (0.3)	1.3

Table 4. Complex refractive indices of individual minerals used in this study. The spectral domains are indicated. *Longtin et al. (1988) have compiled values of complex refractive indices for hematite and quartz based on different sources.

Mineral	Reference	Spectral domain (μm)
Illite	Egan et Hilgeman (1979)	0.185–2.6
	Querry (1987)	2.5–200
Kaolinite	Glotch et al. (2007)	5–100
	Egan et Hilgeman (1979)	0.185–2.6
	Roush et al. (1991)	5–25
Calcite	Glotch et al. (2007)	5–100
	Querry (1978)	0.2–25
Dolomite	Long et al. (1993)	2.5–300
	Barthelmy (2007)	0.185–2.5
Albite	Querry (1987)	2.5–40
	Barthelmy (2007)	0.185–2.5
Orthose	Barthelmy (2007)	0.185–2.5
Gypsum	Barthelmy (2007)	0.185–2.5
Goethite	Long et al. (1993)	2.5–300
	Bedidi et Cervelle (1993)	0.46–0.7
Hematite	Glotch et Rossman (2009)	8.3–50
	Bedidi et Cervelle (1993)	0.4–0.7
	Marra et al. (2005)	6.5–50
Quartz	Longtin et al. (1988)*	0.2–300
	Longtin et al. (1988)*	0.2–2
	Peterson et Weinman (1969)	5–36
	Spitzer et Kleinman (1961)	5–37

Mapping the physico-chemical properties of mineral dust

P. Formenti et al.

[Title Page](#)

[Abstract](#) | [Introduction](#)

[Conclusions](#) | [References](#)

[Tables](#) | [Figures](#)

[⏪](#) | [⏩](#)

[◀](#) | [▶](#)

[Back](#) | [Close](#)

[Full Screen / Esc](#)

[Printer-friendly Version](#)

[Interactive Discussion](#)



Mapping the physico-chemical properties of mineral dust

P. Formenti et al.

Title Page

Abstract

Introduction

Conclusions

References

Tables

Figures

◀

▶

◀

▶

Back

Close

Full Screen / Esc

Printer-friendly Version

Interactive Discussion

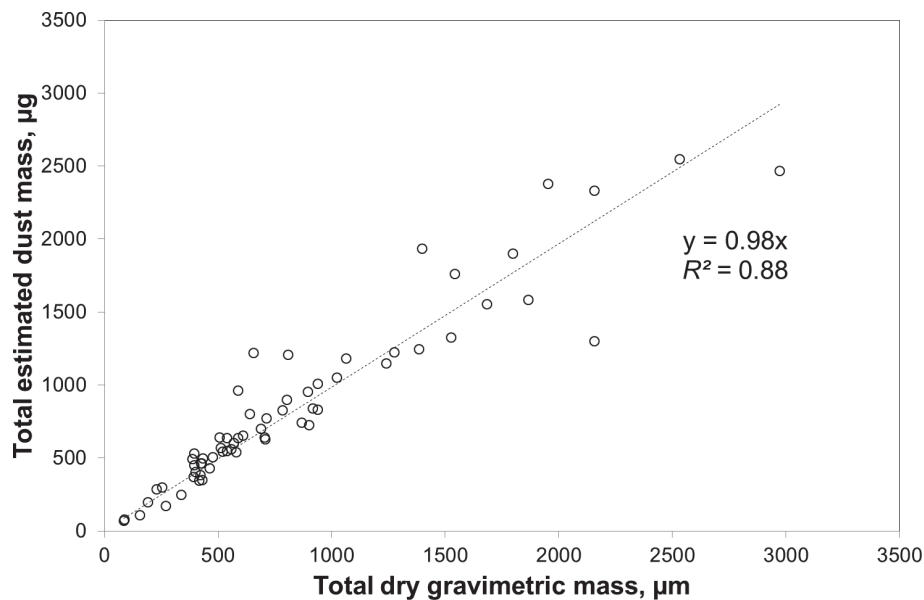


Fig. 1. Comparison between the total estimated dust mass (TEDM) estimated from the chemical composition and the total dry gravimetric mass (TDGM).

Mapping the
physico-chemical
properties of mineral
dust

P. Formenti et al.

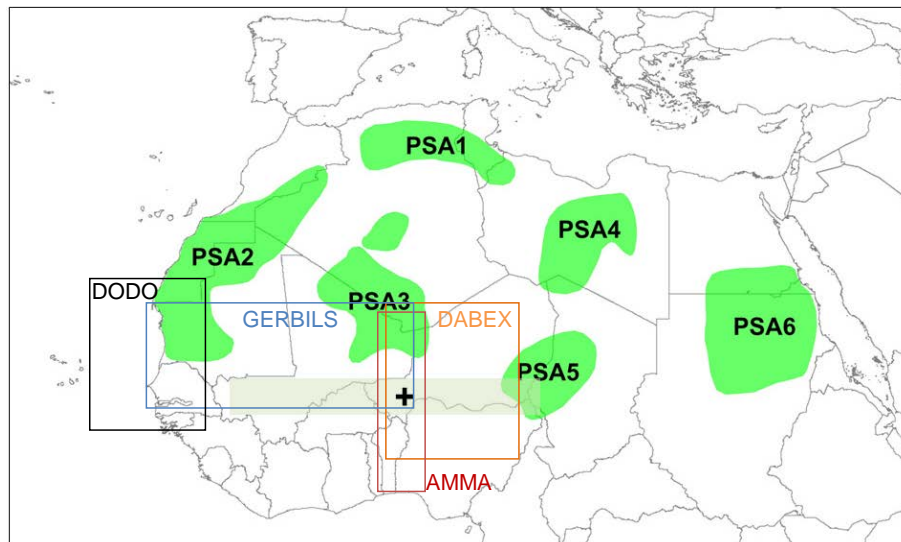


Fig. 2. Geographical identification of the origin of the analysed samples superimposed to the localisation of the major potential source areas (PSA) of mineral dust in western and northern Africa proposed by Formenti et al. (2011a) and Scheuvens et al. (2013) on the basis of the analysis of satellite products and chemical/mineralogical composition on the aerosol and the parent soil (Claquin et al., 1999; Brooks and Legrand, 2000; Caquineau et al., 2002; Prospero et al., 2002; Washington et al., 2003; Schepanski et al., 2007, 2009, 2012; Laurent et al., 2008; Klüser and Schepanski, 2009). The approximate localisation of the Sahelian dust sources is also indicated by the shed grey area. The location of the Banizoumbou ground-based site is indicated by the black cross. The operating areas of the AMMA, DABEX, DOD and GERBILS field projects are shown. Figure reproduced from Scheuvens et al. (2013) with permission from Elsevier.

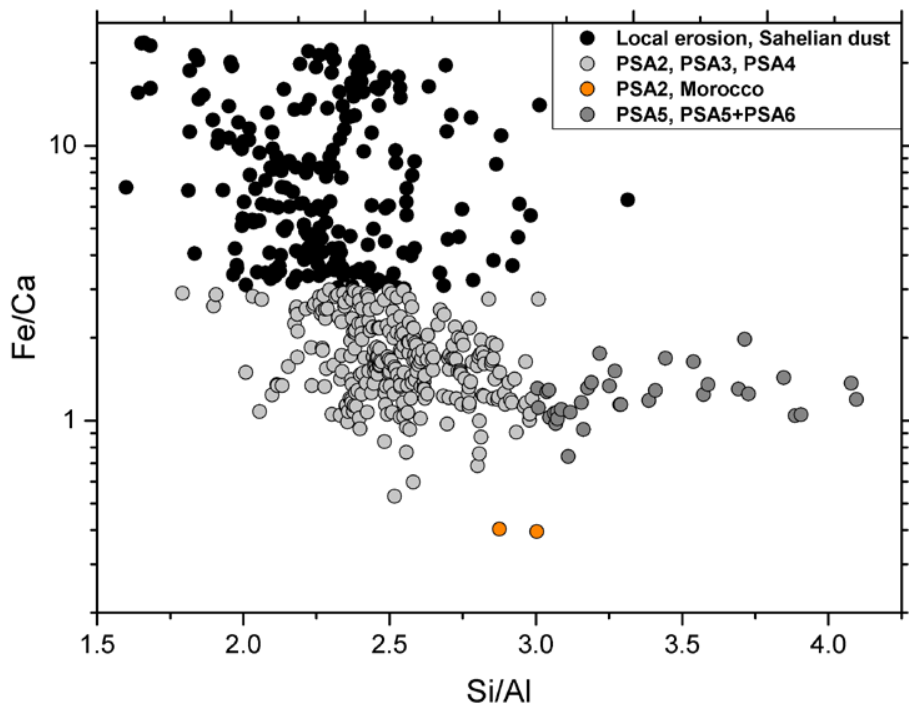


Fig. 3. Scatterplot of the elemental ratio Fe/Ca vs. Si/Al with additional information on source identification based on back-trajectory/satellite and dispersion modeling.

Mapping the physico-chemical properties of mineral dust

P. Formenti et al.

Title Page

Abstract Introduction

Conclusions References

Tables Figures

⏪ ⏩

⏴ ⏵

Back Close

Full Screen / Esc

Printer-friendly Version

Interactive Discussion



**Mapping the
physico-chemical
properties of mineral
dust**

P. Formenti et al.

Title Page

Abstract

Introduction

Conclusions

References

Tables

Figures



Back

Close

Full Screen / Esc

Printer-friendly Version

Interactive Discussion

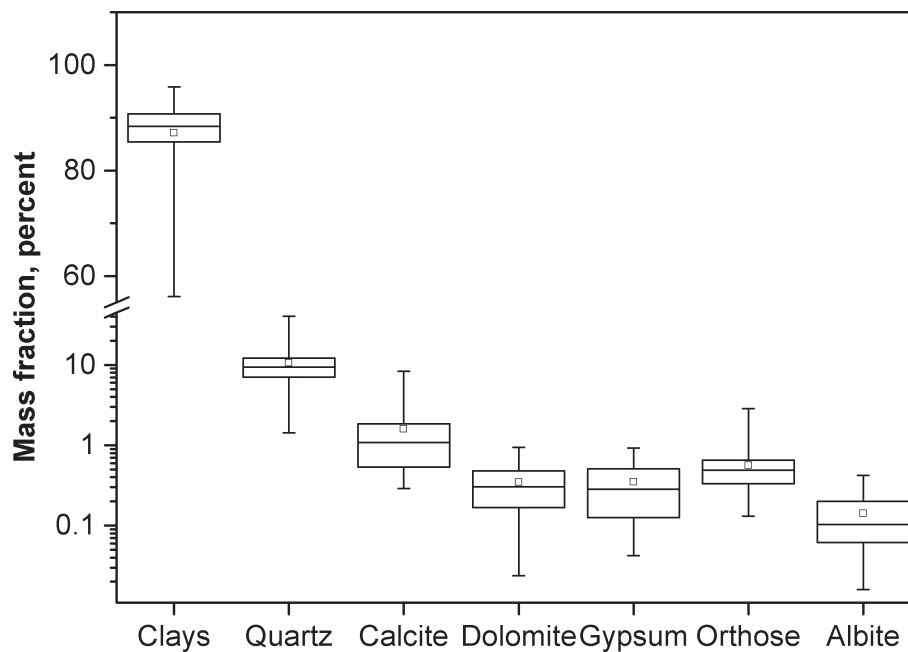


Fig. 4. Range of variability of the mineral mass fraction (in percent) as obtained by XRD analysis. Boxes indicate the 25, 50 and 75 % percentiles. Whiskers indicate the minimum and the maximum values, whereas the open squares indicate the mean value of the distribution.

Mapping the physico-chemical properties of mineral dust

P. Formenti et al.

Title Page

Abstract

Introduction

Conclusions

References

Tables

Figures

⏪

⏩

◀

▶

Back

Close

Full Screen / Esc

Printer-friendly Version

Interactive Discussion

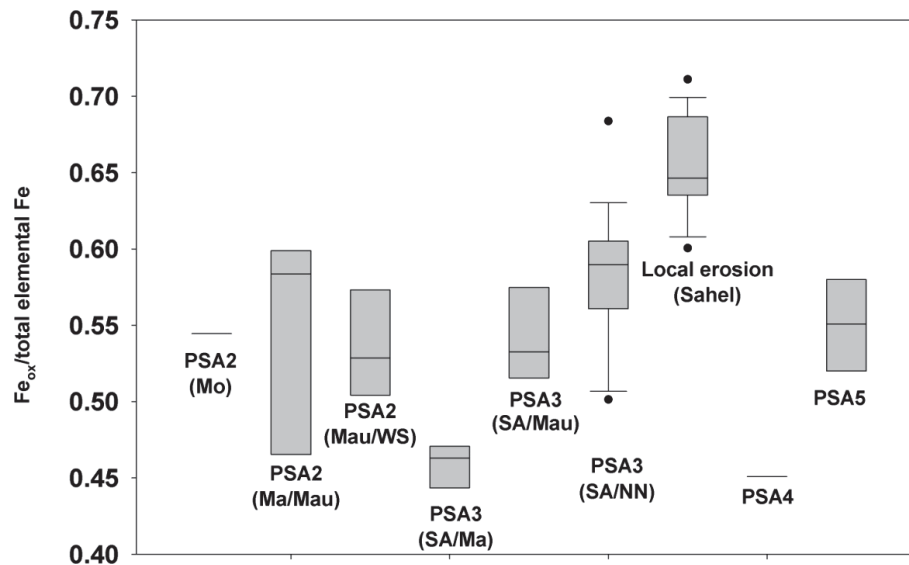


Fig. 5. Variability of the iron oxide content (ratio of Fe_{ox} to total elemental Fe) according to the source region. Boxes indicate the 25, 50 and 75 % percentiles. Points indicate the minimum and the maximum values, and Whiskers indicate the 5 and 95 % percentiles. Data labels are as follows: Mo = Morocco; Ma = Mali; Mau = Mauritania; SA = South Algeria; NN = North Niger.

Mapping the physico-chemical properties of mineral dust

P. Formenti et al.

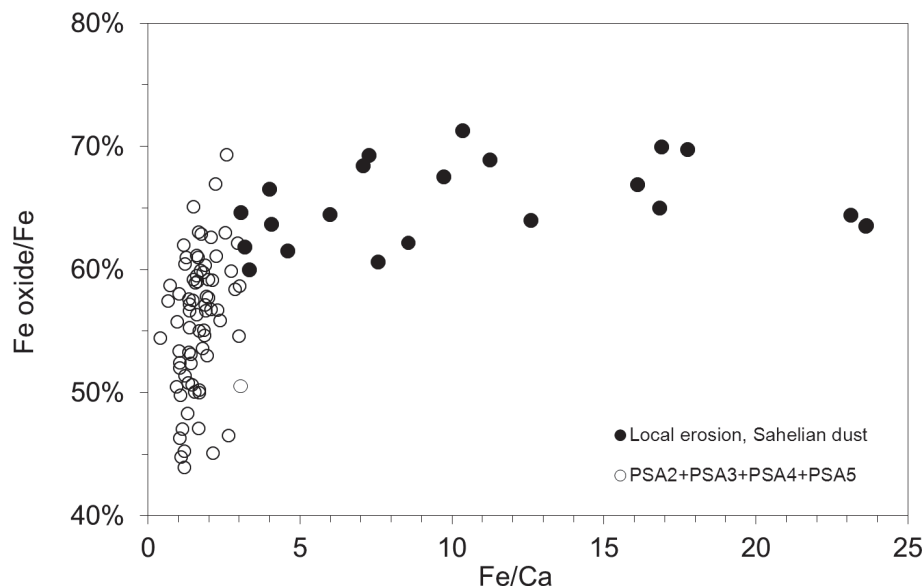


Fig. 6. Dependence of the Fe_{ox} content (Fe_{ox}-to-Fe ratio) on the Fe/Ca ratio for samples of different source regions identified in this work.

Mapping the
physico-chemical
properties of mineral
dust

P. Formenti et al.

Title Page

Abstract

Introduction

Conclusions

References

Tables

Figures

◀

▶

◀

▶

Back

Close

Full Screen / Esc

Printer-friendly Version

Interactive Discussion

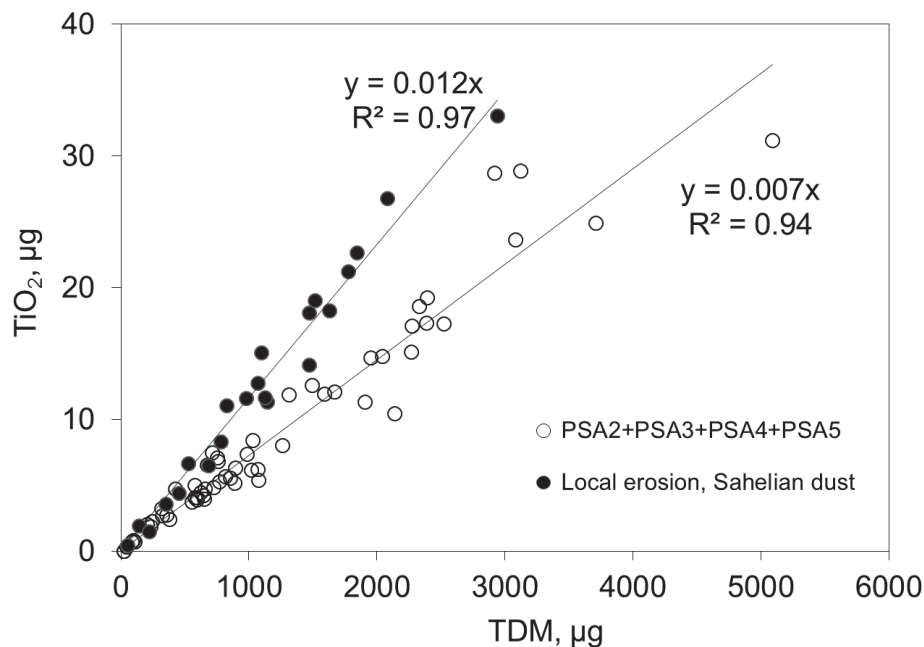


Fig. 7. Scatterplot of the estimated mass of TiO_2 with respect to the total dust mass (TDM). Open circles are used to display values for samples corresponding to transport of Saharan dust, whereas filled circles are for samples corresponding to local emission in the Sahel.

Mapping the physico-chemical properties of mineral dust

P. Formenti et al.

Title Page

Abstract

Introduction

Conclusions

References

Tables

Figures

⏪

⏩

◀

▶

Back

Close

Full Screen / Esc

Printer-friendly Version

Interactive Discussion

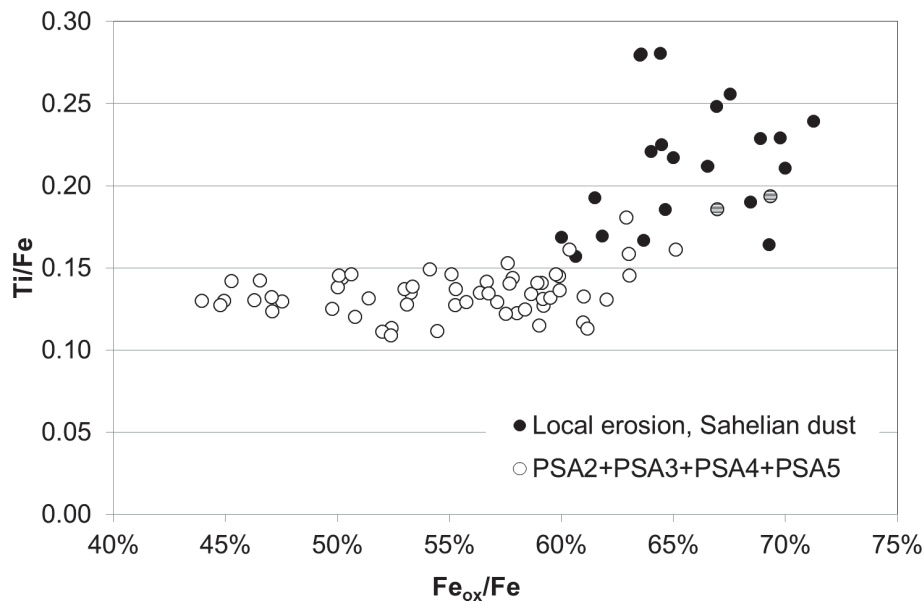


Fig. 8. Scatterplot of the Ti/Fe ratio with respect to the Fe_{ox} -to- Fe ratio. Open circles are used to display values for samples corresponding to transport of Saharan dust, whereas filled circles are for samples corresponding to local emission in the Sahel. Two grey points indicates identified mixtures.

**Mapping the
physico-chemical
properties of mineral
dust**

P. Formenti et al.

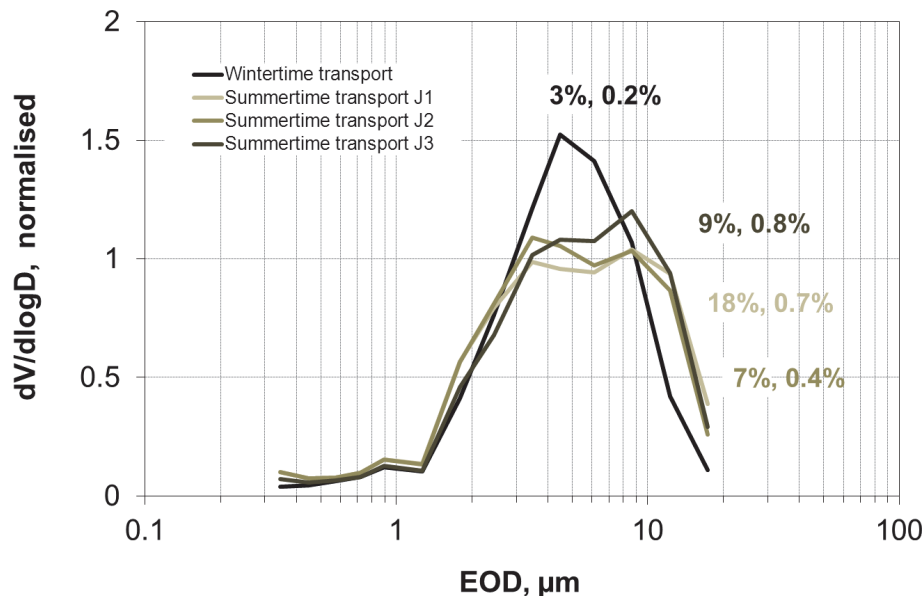


Fig. 9. Volume size distribution $dV/d\log(EOD)$, normalised to the total volume, for samples representing dust transported to the Banizoumbou site from the Bodélé source region. In summertime, transport was monitored on three consequent days, indicated as J1, J2 and J3, respectively. Data are reported as a function of the equivalent optical diameter (EOD) as obtained by optical counter measurements without any corrections for the sample refractive index. Numbers represent the measured percent mass fraction of quartz and feldspars (sum of albite and orthose), respectively.

Mapping the physico-chemical properties of mineral dust

P. Formenti et al.

Title Page

Abstract

Introduction

Conclusions

References

Tables

Figures

◀

▶

◀

▶

Back

Close

Full Screen / Esc

Printer-friendly Version

Interactive Discussion

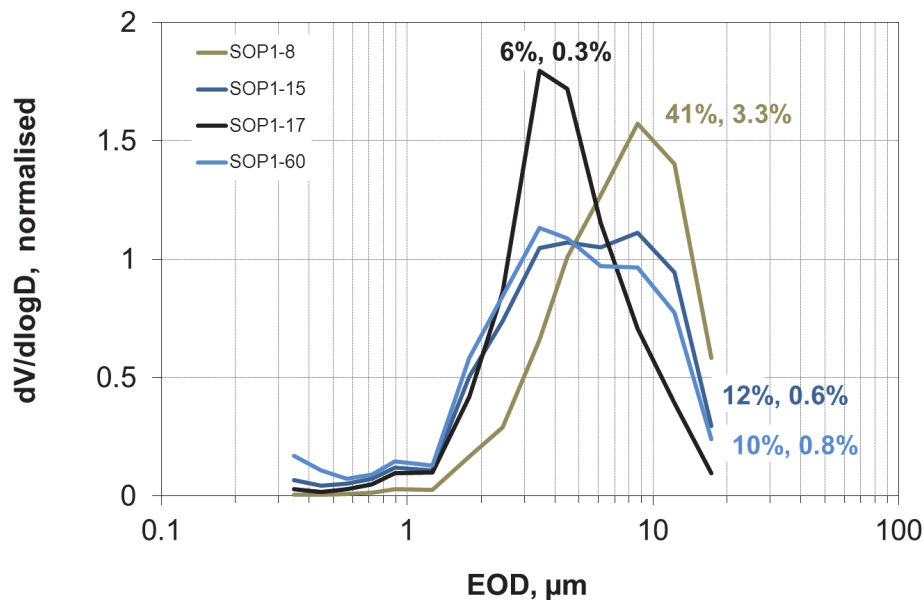


Fig. 10. Volume size distribution $dV/d\log(EOD)$, normalised to the total volume, for samples representing Sahelian dust: SOP1-8 representing an episode of local emission by erosion; SOP1-15 and SOP1-60 representing the background dust composition in the absence of local erosion; and SOP1-17 representing the composition of Sahelian dust advected at the sampling site after having been emitted by local erosion in the proximity. Numbers represent the measured percent mass fraction of quartz and feldspars (sum of albite and orthose), respectively.

Mapping the physico-chemical properties of mineral dust

P. Formenti et al.

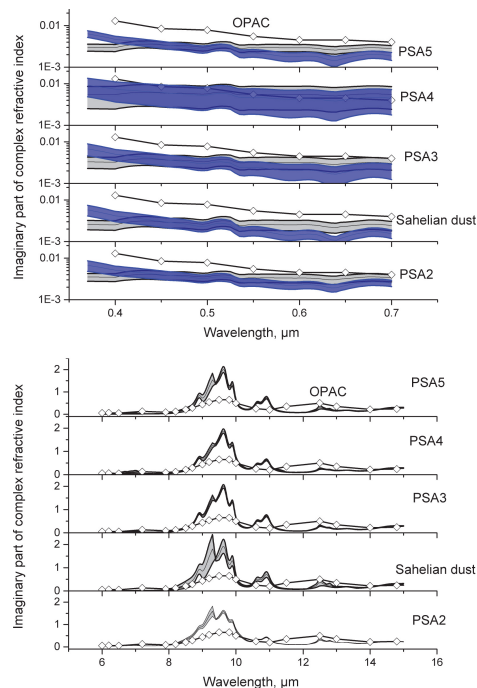


Fig. 11. Imaginary part of the complex refractive index calculated from the mineralogical composition of dust steaming from sources PSA5, PSA4, PSA3, local erosion in the Sahel, and PSA2 (from top to bottom). **(a)** represents the real part in the 0.3–0.7 μm , calculated assuming refractive index from Table 3. Grey shaded curves represent the mean values (light grey line) and 1 standard deviation (grey shaded areas) obtained when using the data from Bedidi and Cervelle (1993) for hematite, whereas blue shaded areas correspond to values calculated using the hematite data from Shettle (1979). The light blue line represents mean values and the blue shaded area represents one standard deviation. **(b)** represents the imaginary part of the complex refractive index calculated in the 6–16 μm spectral domain. The black line with white diamonds represents data from the OPAC database (Hess et al., 1998).

Mapping the physico-chemical properties of mineral dust

P. Formenti et al.

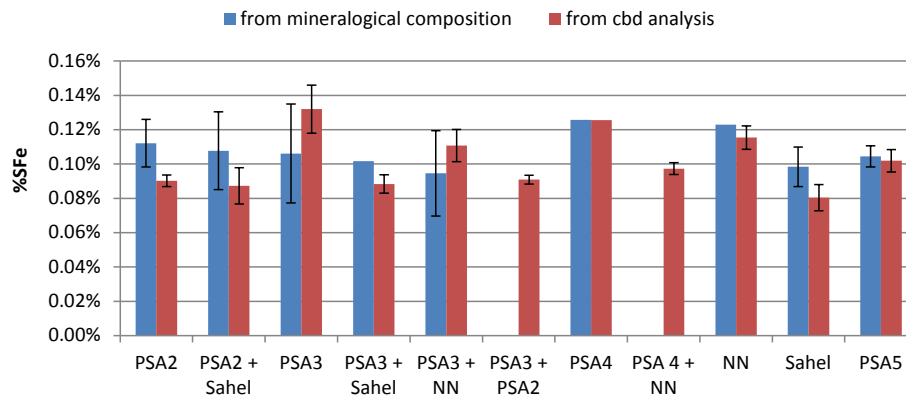


Fig. 12. Iron solubility calculated from the mineralogical composition and from CBD analysis as a function of emission source. Error bars indicate standard deviation. When error bar is not presented, the data is only for one sample.

Title Page

Abstract

Introduction

Conclusions

References

Tables

Figures

⏪

⏩

◀

▶

Back

Close

Full Screen / Esc

Printer-friendly Version

Interactive Discussion